ORGANOMETALLICS
Article
Cite This: *Organometallics* XXXX, XXX, XXX−XXX
pubs.acs.org/Organometallics

C−H Nickelation of Naphthyl Phosphinites: Electronic and Steric Limitations, Regioselectivity, and Tandem C−P Functionalization

Loïc P. Mangin and Davit Zargarian*

Département de Chimie, Université de Montréal, Montréal, Québec H3C 3J7, Canada

Supporting Information

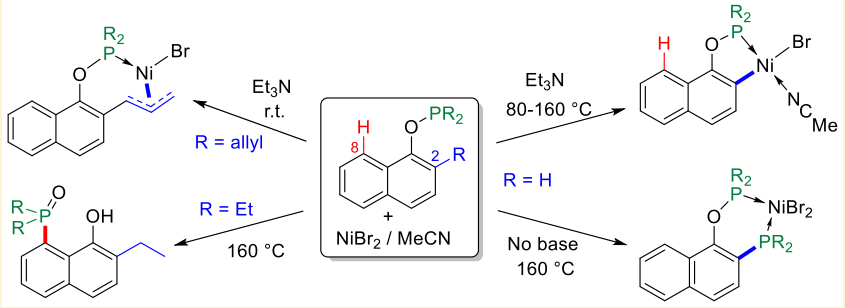

ABSTRACT: This report describes the results of a study on the C−H nickelation of phosphinites derived from variously substituted 1- and 2-naphthols, as well as the C−P functionalization of the Ni-naphthyl moiety arising from the C−H cyclonickelation. Refluxing 4-X-1-naphthyl phosphinites (X = H, **1a**; MeO, **1b**; Cl, **1c**) with $\{(i\text{-PrCN})NiBr_2\}_n$ and Et_3N in acetonitrile gave the nickelacyclic complexes $\{(\kappa^P,\kappa^C\text{-4-X-1-OP}(i\text{-Pr})_2\text{-naphth-2-yl})Ni(\mu\text{-Br})\}_2$, **2a−c**, resulting from cyclonickelation at the C2−H, whereas cyclonickelation of the 2-naphthyl phosphinite analogue **1e** under the same conditions occurred at C3−H. Placing a Me substituent at the C3 position of a 2-naphthyl phosphinite (**1f**) led to a very sluggish nickelation at the C1−H position, whereas 2-ethyl-1-naphthyl phosphinite (**1d**) failed to nickelate at C8−H. H/D scrambling tests conducted on the deuterated analogue of **1a** (**1a**-d_7) confirmed that nickelation occurs exclusively at C2. Similar tests conducted on deuterated analogues of alkyl-substituted 1- and 2-naphthyl phosphinites showed that no nickelation takes place at C_{sp^3}−H sites of the alkyl substituents. In contrast, very facile C−H nickelation was observed with 2-allyl-1-naphthyl phosphinite **1g** to give a product featuring a π-allyl-Ni moiety. A series of tests have shown that the nickelation of substrates **1a**, **1e**, and **1f** can be accelerated dramatically at 120−160 °C. On the other hand, conducting the high temperature reaction of **1a** in the absence of Et_3N resulted in an unanticipated and interesting C−P functionalization of the C2−H site, thus generating a *i*-Pr_2P-substituted bidentate phosphine-phosphinite. A similar tandem C−H nickelation/C−P(O) functionalization was also observed at the C8−H position of substrate **1d**. The mechanisms of these functionalization reactions have been probed and outlined.

INTRODUCTION

Catalytic processes based on non-redox-type C−H metalation and tandem functionalization have gained increasing prominence in the drive toward sustainable chemical synthesis.[1] Historically, the early success of these processes was due in large part to the use of noble metal-based precursors, and to some extent the supremacy of these metals persists today.[2] However, the past decade has witnessed the development of many efficient C−H functionalization processes that are catalyzed by precursors based on the more abundant 3d metals.[3] In addition to the potential cost advantages of the latter relative to their 4d and 5d congeners, continued investigations of C−H metalation-functionalization chemistry based on 3d metals also open the door to the discovery of new and complementary reactivity patterns, which can be exploited to create exciting opportunities in commercial developments.

Our group's contributions to this field have focused on the C−H nickelation of phosphinites derived from phenol and its substituted derivatives. In an initial report, we showed that orthometalation of $ArOP(i\text{-Pr})_2$ is feasible with the Ni(II) precursor $\{(i\text{-PrCN})NiBr_2\}_n$.[4] The isolation and structural characterization of the resulting cyclonickelated species have allowed us to gain some understanding of their thermal stabilities and reactivities in C−C and C−heteroatom functionalization (Scheme 1, **A**).

We have also delineated the impact of reaction solvent, external base, and aryl substituents on the kinetics and energetics of C−H nickelation.[5] It was found, for instance, that C−H bond rupture is rate determining ($k_H/k_D \approx 11$), and that nickelation proceeds faster with substrates bearing electron-releasing substituents.[6] Significantly, D-labeling studies and rate measurements indicated that the C−H nickelation step occurs reversibly and independently of the presence of an

Received: October 7, 2019

DOI: 10.1021/acs.organomet.9b00660
Organometallics XXXX, XXX, XXX−XXX

Scheme 1. C−H Nickelation with Aryl Phosphinites

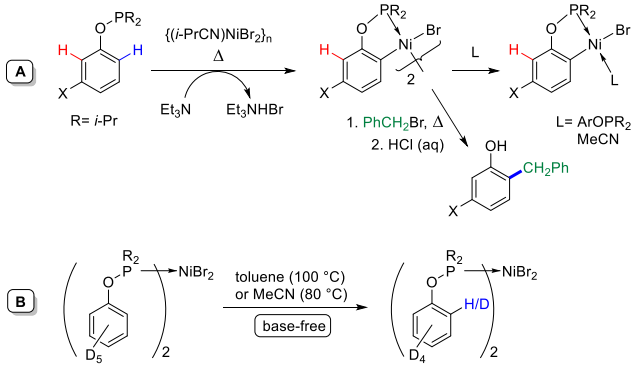

external base (Scheme 1, **B**). On the other hand, *isolation* of the nickelacyclic complex resulting from the C−H metalation step requires a sufficiently strong external base, because the acid generated during the nickelation step protonates the newly formed Ni-aryl moiety to reverse the C−H nickelation.[5] Finally, studying the C−H nickelation of aryl phosphinites based on 3-substituted phenols has revealed that the regiochemistry of orthonickelation is strongly influenced by steric factors.[6]

In continuation of our previous investigations, we have begun to examine the C−H nickelation of phosphinites derived from 1- and 2-napththols. These substrates offer two potentially reactive C−H sites, but the steric and electronic properties of these sites of reactivity are more dissimilar than in phosphinites derived from phenol. For instance, nickelation of 1-naphthyl phosphinite at C2 would give a 5-membered nickelacycle, whereas reaction at C8 would generate a 6-membered nickelacycle. In the case of 2-naphthyl phosphinite, nickelation at both *ortho* C−H sites (C1 and C3) would generate 5-membered nickelacycles, but these two products would be reasonably expected to display different reactivities based on their steric and electronic differences.

There is scant literature on the metalation of naphthyl phosphinites, but the few precedents that do exist offer us an indication of which C−H site might be more favorable to metalation. Bedford has shown, for example, that metalation of 1-naphthyl phosphinites with Rh occurs mainly at the C2−H site, but it can also take place to a lesser extent at the C8 site to give a 6-membered rhodacycle.[7] The analogous reactivity with 2-naphthyl phosphinites takes place at both C1−H and C3−H sites.[9] In the case of Pd, metalation of 1-naphthoxide (as opposed to its phosphinite) has been reported to occur at C8−H, whereas palladation of 2-naphthoxides takes place exclusively at C1, presumably generating a 4-membered palladacycle.[8] The above considerations prompted us to study the nickelation of naphthyl phosphinites and compare the results to the nickelation of phenyl phosphinites.

The present contribution reports the cyclonickelation of 1- and 2-naphthyl phosphinites and some of their substituted derivatives. We have found that nickelation of 1-naphthyl phosphinites occurs at C2 in preference over C8, whereas the C3 site is favored over C1 for 2-naphthyl phosphinites. In the latter case, blocking the favored pathway allowed us to induce nickelation at the less favored C1−H site, but a similar strategy was much less successful for 1-naphthyl phosphinite. In some cases, conducting the reactions at high temperatures led to accelerated C−H nickelation rates and a potentially useful tandem C−P functionalization.

RESULTS AND DISCUSSION

C−H Nickelation of 1-Naphthyl Phosphinites. Our studies began by examining the reactivities of 1-naphthyl phosphinites under the reaction conditions optimized for the C−H nickelation of substrates derived from substituted phenols. Thus, the substrate being studied was refluxed in acetonitrile in the presence of $\{(i\text{-PrCN})NiBr_2\}_n$ and Et_3N, the latter serving the purpose of quenching the HBr generated in situ at the C−H nickelation step. Scheme 2 shows the acetonitrile adducts of the cyclonickelated products generated from 1-naphtyl phosphinites **1a**−**1c**.

Scheme 2. Nickelation of 4-X-1-Naphthyl Phosphinites

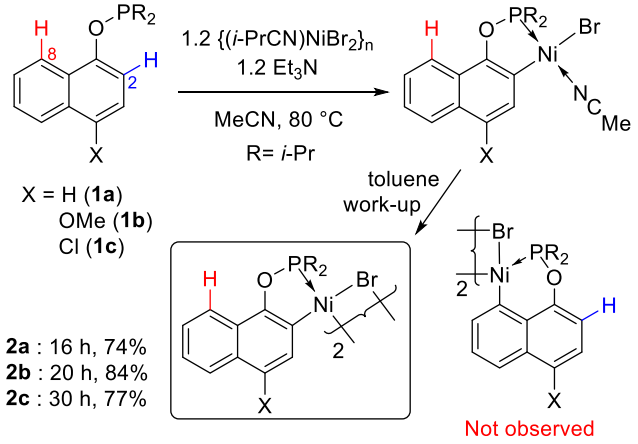

Complete conversions took place over 16−30 h, which was confirmed by the ^{31}P NMR spectra of the final reaction mixtures displaying new singlet resonances at 194−197 ppm, the chemical shift region characteristic of cyclonickelated $ArOP(i\text{-Pr})_2$.[5] The green reaction mixtures containing the cyclonickelated products were then worked up in toluene to give the target dimeric complexes as orange powders in 74−84% isolated yields. Complete characterization of **2a**−**2c** by NMR and single crystal XRD confirmed that the desired cyclonickelation had taken place at the C2 to give 5-membered nickelacycles (Figure 1); the putative compounds arising from nickelation at the C8 position and featuring 6-membered nickelacycles were not observed.

The solid-state structures of **2a**−**c** will be discussed in the last section of this report, but the reaction times required for their formation and the isolated yields merit some comment

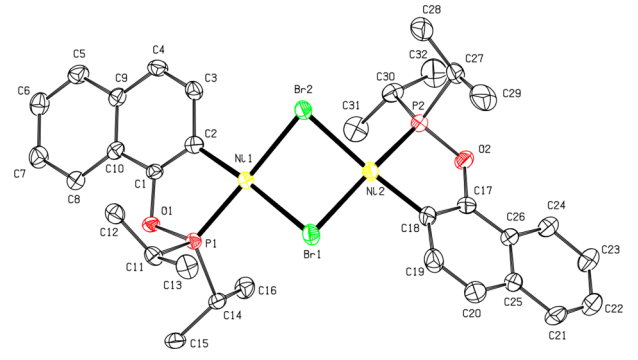

Figure 1. Top view of the molecular diagram for complex **2a**. Thermal ellipsoids are shown at the 50% probability level; hydrogens are omitted for clarity.

DOI: 10.1021/acs.organomet.9b00660
Organometallics XXXX, XXX, XXX−XXX

here. The yields obtained for complexes **2a**−**2c** are somewhat higher than those obtained for the analogous dimeric complexes derived from phenol (67%), 3-MeO-phenol (60%), and 3-Cl-phenol (71%). We believe that these higher yields are due to the lower solubility of these complexes in Et_2O and hexanes, which facilitates product isolation by precipitation from these solvents.

As for the different reaction times required for the formation of **2a**−**2c**, although we have not made systematic measurements of reaction rates in this study, monitoring the ^{31}P NMR spectra of the reaction mixtures showed that the nickelation times varied as a function of substituents X, going to completion within 20 h for X = H and OMe, but requiring longer times for X = Cl. The observation of faster nickelation for **2a** and **2b** echoes our previous results on the faster nickelation of aryl phosphinites bearing electron-rich substrates (Hammett slope of ca. −4).[6]

The observation of exclusive nickelation at C2 for **1a**−**1c** prompted us to ask if the nickelation can be forced to occur at the alternative C8 site. This was examined by testing the C−H nickelation of 2-Et-1-naphthyl phosphinite, **1d**,[9] in which the C2 site is blocked by a substituent. This substrate was subjected to the standard cyclonickelation conditions at 80 °C for 3 days, to no avail: analysis of the final reaction mixture by ^{31}P NMR spectroscopy showed no signal in the 190−210 ppm range, implying no nickelation (Scheme 3).

Scheme 3. Inertness of 2-Ethyl-1-Naphthyl Phosphinite toward Nickelation

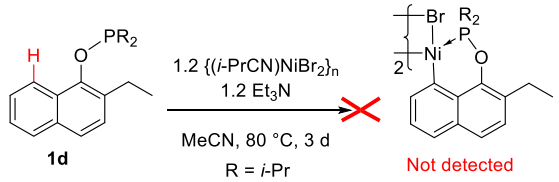

The issue of cyclonickelation regioselectivity with 1-naphthyl phosphinites, i.e., reactivity at C2 vs C8 sites, was further examined using H/D scrambling experiments. This idea was inspired from H/D scrambling experiments we carried out in a previous study on the cyclonickelation mechanism of aryl phosphinites.[6] Thus, heating $C_6D_5OPR_2$ and $\{(i\text{-PrCN})NiBr_2\}_n$ in CH_3CN or protio-toluene *in the absence of external base* led to partial incorporation of H into the *ortho* C−D sites of the phosphinite (Scheme 1, **B**). This allowed us to conclude that nickelation occurs independently of external base, but the in situ generated DBr can undergo D/H exchange with the solvent to generate HBr, which then protonates the cyclonickelated species to generate 2-H-$C_6D_4OPR_2$ (reversible nickelation).

By analogy to the above approach, we set out to conduct a D/H scrambling experiment aimed at establishing whether nickelation of 1-naphthyl phosphinite might be taking place at the C8−H position. To do this, we prepared 1-naphthyl-d_7-$OP(i\text{-Pr})_2$ (**1a-d_7**)[9] and used it to prepare the precursor complex *trans*-$\{(1\text{-naphthyl-}d_7\text{-}OP(i\text{-Pr})_2\}_2NiBr_2$ (**3a-d_7**), which was subsequently heated in CH_3CN for 1 day at 80 °C (Scheme 4).

Cooling the final reaction mixture to −35 °C allowed us to isolate the product by crystallization, and ^1H NMR analysis in $CDCl_3$ revealed 53% H-incorporation into the C2 position (Figure S137).[10] H-incorporation into C8 was not detected

Scheme 4. Testing D/H Scrambling in 1-Naphthyl Phosphinite

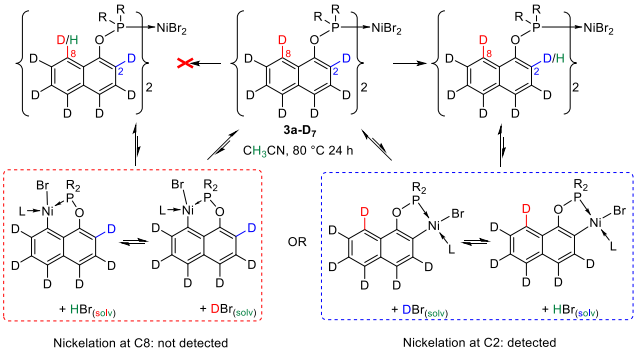

even after 3 days of heating. This establishes that the formation of the expected 6-membered nickelacycle is either kinetically not allowed in these conditions or, if nickelation does take place at C8−H, the in situ generated DBr reacts with the resulting Ni−C moiety to reverse nickelation faster than D/H exchange with the solvent.

C−H Nickelation of 2-Naphthyl Phosphinites. Cyclonickelation of 2-naphthyl phosphinite, **1e**, proceeded even more sluggishly than the analogous nickelation of 1-naphthyl phosphinites **1a**−**1c**, requiring 60 h at 80 °C to go to completion (Scheme 5). Nevertheless, the ^{31}P NMR spectrum

Scheme 5. Nickelation of 2-Naphthyl Phosphinite

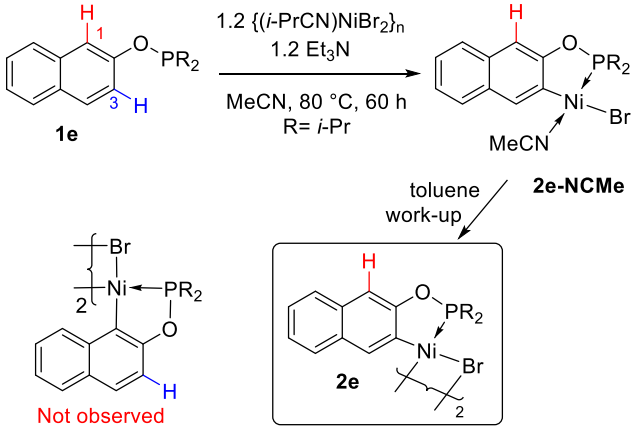

of the final reaction mixture confirmed a clean conversion of **1e** to a new species displaying a singlet at 197 ppm. Cooling the reaction mixture to room temperature gave yellow crystals, which were identified by XRD analysis as the acetonitrile adduct of the cyclonickelated compound (**2e-NCMe** in Scheme 5).

On the other hand, isolation of the corresponding dimeric complex **2e** by the usual workup protocol was hampered by its limited solubility in toluene. Conducting the extraction process using hot toluene dissolved more of **2e-NCMe**, thus allowing us to isolate **2e** with ca. 54% yield. However, despite multiple attempts to purify the crops of **2e** obtained from this approach, they always contained residual toluene impurities, whereas pure samples of the acetonitrile adduct **2e-NCMe** could be obtained from these in 80% yield.

C−H nickelation of **1e** could, in principle, occur at one of the two *ortho* C−H positions C1 and C3, but NMR characterization and XRD analyses of **2e** and **2e-NCMe**

DOI: 10.1021/acs.organomet.9b00660
Organometallics XXXX, XXX, XXX−XXX

revealed C3 to be the only site of reactivity (Scheme 5, Figure 2).

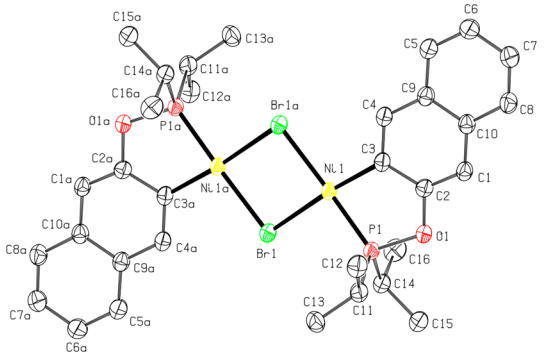

Figure 2. Top view of the molecular diagram for complex **2e**. Thermal ellipsoids are shown at the 50% probability level; hydrogens are omitted for clarity.

This raised the question of whether the observed preference for nickelation at C3 vs C1 originates from steric or electronic factors. Our previous investigations on the nickelation of phosphinites derived from 3-R-phenols had demonstrated that electronic factors can influence nickelation rates but not regioselectivity, whereas steric hindrance is the main determinant of which C−H is nickelated.[11,12] By analogy, it seems reasonable to conclude that the observed preference for nickelation of **1e** at C3 must be due to lower steric hindrance at this site relative to C1. On the other hand, the much *slower* nickelation of this substrate compared to the analogous reactions with 1-naphthyl phosphinites **1a**−**1c** is likely caused by unfavorable electronic factors, the C3 position in 2-naphthols being less electron-rich relative to the C1 position.[13]

Similarly to the above-described probe of regioselectivity with substrate **1d** (Scheme 3), we examined the C−H nickelation of 3-Me-2-naphthyl phosphinite, **1f**, in which the more reactive C3 site has been blocked in order to see if C−H nickelation can be forced to occur at the less favored C1 site (Scheme 6).

Refluxing the emerald green acetonitrile mixture resulting from mixing **1f** with $\{(i\text{-PrCN})NiBr_2\}_n$ and Et_3N led to formation of a new species, but complete conversion was not achieved even after 10 days. NMR monitoring of the reaction progress showed a new ^{31}P singlet at ca. 192 ppm, which we tentatively assign to **2f-NCMe** (Scheme 6). Integrating this peak against that of the internal standard $[n\text{-}Bu_4N][PF_6]$ showed conversions of about 10% and 16% after 3 and 7 days, respectively. Unfortunately, the standard workup of the reaction mixture in toluene was complicated by the presence of significant quantities of the unreacted starting material; as a result, we obtained only a small quantity of crystals. Nevertheless, XRD analysis conducted on these crystals showed that this reaction generated a phosphinite adduct of the cyclonickelated species **2f-L** wherein nickelation of **1f** had taken place at C1 (Scheme 6).

Scheme 6. Nickelation of the 3-Me-2-Naphthyl Phosphinite 1f and Molecular Diagram[a] of 2f-L

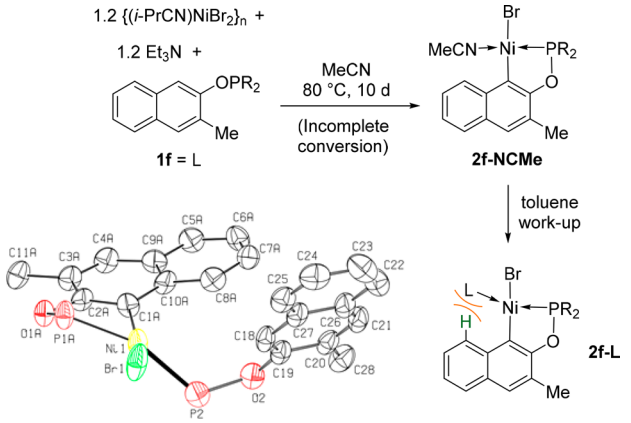

[a]Thermal ellipsoids are shown at the 50% probability level; hydrogens and *P*-substituents are omitted for clarity.

Comparison of the C−H nickelation regioselectivities observed for the 2-naphthyl phosphinites **1e** and **1f** and the relative facility/sluggishness of these reactions inform us on the relative importance of sterics and electronics for these reactions. Thus, in substrate **1e** wherein C−H nickelation is, in principle, possible at both sites, reactivity takes place at C3 in preference over the more electron-rich C1 site; moreover, the nickelation of this substrate required 60 h. In contrast, with substrate **1f** wherein the C3 site is blocked by the Me substituent, the nickelation occurred at the alternative C1 site, but at a very sluggish pace.

We believe that the sluggishness of nickelation with **1f** results from the steric congestion at the C1 site. Consistent with this, the molecular diagram of **2f-L** (Scheme 6) revealed a very distorted structure in which the steric repulsion between C8−H and the phosphinite has caused a significant twist around the Ni−C1 axis. Indeed, the tetrahedral distortion parameter τ_4[14] around the Ni center was found to be 0.30−0.35, caused primarily by the out-of-plane displacement of the non metalated naphthyl phosphinite ligand. As a result, the dihedral angle of ca. 50° for C10A−C1A−Ni1−P2 represents a significant out-of-plane rotation of the nickelated naphthyl ring.

Reactivity of Ortho Substituents. In the above discussions on the regioselectivity of C−H nickelation with alkyl-substituted 1- and 2-naphthyl phosphinites, the possibility of nickelation at the alkyl substituents was not considered. Discounting this possibility might be justified, because metalation of C_{sp^3}−H bonds is usually more difficult, and the resulting Ni−C_{sp^3} bonds are known to be less stable than Ni−C_{sp^2} bonds arising from metalation of C_{sp2}−H. Nevertheless, it seemed important to determine if C_{sp^3}−H nickelation can be kinetically accessible in naphthyl phosphinites bearing *ortho*-alkyl substituents. We have probed this possibility by using a H/D scrambling test analogous to the one shown in Scheme 4 for studying C−H nickelation at C8 in **1a**.

Stirring the deuterated analogue of **1d** with $\{(i\text{-PrCN})\text{-}NiBr_2\}_n$ in dichloromethane at r.t. gave the target compound $\{2\text{-}CH_3CD_2\text{-}1\text{-naphthyl-OP}(i\text{-Pr})_2\}_2NiBr_2$,[9] **3d-*d*$_2$** (Scheme 7). Refluxing the latter in acetonitrile or toluene over extended reaction times (up to 3 days), followed by gradual cooling to −35 °C gave crystals after 1 day. Analysis of these crystals by ^1H NMR ($CDCl_3$) confirmed that no H-incorporation had taken place into the α C_{sp^3}−D positions (Scheme 7). The analogous scrambling test was also conducted for the deuterated analogue of **1f**,[9] with the same results: ^1H NMR analysis of crystals of **3f-*d*$_3$** obtained after heating showed no H-incorporation into the α C_{sp^3}−D site (Scheme 7). We conclude, therefore, that nickelation of the $C_{sp^3}H(D)$ sites in

DOI: 10.1021/acs.organomet.9b00660
Organometallics XXXX, XXX, XXX−XXX

Scheme 7. D/H Scrambling Tests with 1- and 2-Phosphinites Bearing α-Deuterated Alkyl Substituents

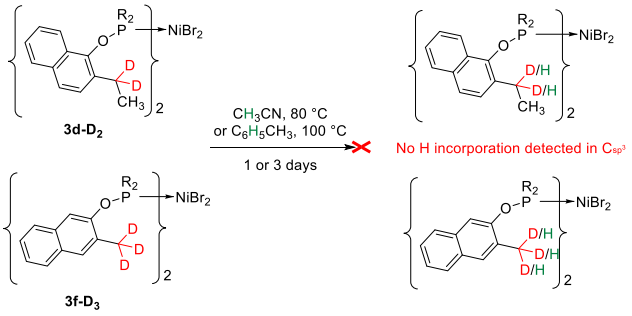

alkyl-substituted 1- or 2-naphthyl phosphinites is either not happening in our system or, if it is, the resulting nickelated product is simply too high in energy and reverts back to its starting form faster than the competing H/D exchange with the solvent.

The observed inertness of the alkyl substituents in **1d** and **1f** prompted us to ask if a more activated allylic/benzylic CH_2 moiety would get nickelated. To answer this question, we prepared substrate **1g**[9] and tested its C−H nickelation with $\{(i\text{-PrCN})NiBr_2\}_n$ and Et_3N (Scheme 8: acetonitrile, 80 °C, 2 h).

Scheme 8. C−H Nickelation of 2-Allyl-1-Naphthyl Phosphinite 1g and Molecular Diagram[a] of 2g

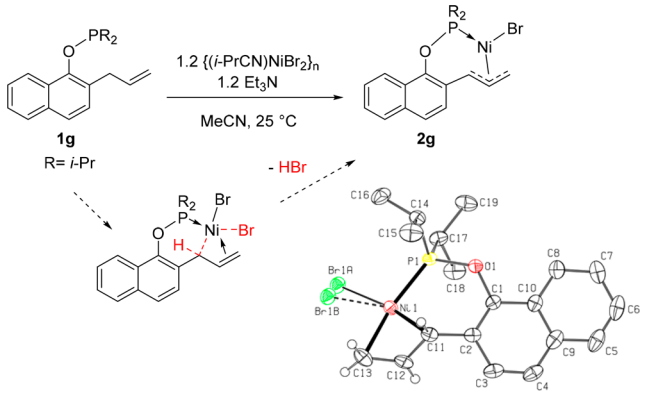

[a]Thermal ellipsoids are shown at the 50% probability level; hydrogens and P substituents are omitted for clarity.

This reaction did give a new species represented by a ^{31}P singlet at 201 ppm, which we ascribed to a nickelated species. However, there were also significant amounts of Ni black deposited on the walls of the reaction flask, implying that some of the putative nickelated complexes are prone to decomposition. Repeating the reaction at lower temperatures allowed us to promote the nickelation while avoiding thermal degradation. For instance, conducting the reaction with 1 equiv of Ni precursor and 2 equiv of Et_3N at r.t. over 16 h led to a cleaner nickelation. Workup of the final reaction mixture followed by crystallization in Et_2O/pentane gave orange crystals that were shown by XRD to be the monomeric complex **2g** featuring an η^3-π-allyl moiety (Scheme 8).

Complex **2g** features a 6-membered nickelacycle with significantly longer Ni−C11 (1.983 and 1.972 Å)[15] and Ni−P bonds (2.145 and 2.134 Å) relative to other dimers featuring 5-membered nickelacycles. Moreover, the allyl moiety is less symmetrical than in "free" π-allyl complexes of Ni(II)Br, and the naphthalene ring bends out of the mean plane around Ni by 25−37°.

Evidently, C−H nickelation at a methylenic C−H in **1g** is feasible and fairly facile, presumably due to the binding of the terminal olefin moiety of the substituent to the Ni(II) center; this would be akin to the C−H nickelation of a LXL′ pincer ligand, which is often more facile than a simple cyclonickelation.[16] Unfortunately, efforts to isolate the putative bidentate phosphinite-olefin intermediate shown in Scheme 8 from 1:1 mixtures of **1g**:$\{(i\text{-PrCN})NiBr_2\}_n$ yielded only the bis-phosphinite L_2NiBr_2 complex (**3g**).

Acceleration of C−H Nickelation at High Temperatures. The generally sluggish rate of C−H nickelation for 1- and 2-naphthyl phosphinites (16 h of refluxing in MeCN in the most favorable case) spurred us to find a way to accelerate these reactions. Tests showed that much faster C−H nickelation is possible with some substrates by conducting the reactions in a thermostated autoclave that allows us to safely attain reaction temperatures above the boiling point of the solvent. For instance, using this approach led to near complete nickelation of **1a** in only 30 min at 160 °C, which is significantly faster than the 16 h required for the analogous nickelation to occur in a Schlenk tube at 80 °C (Scheme 9).

Scheme 9. C−H Nickelation of 1- and 2-Naphthyl Phosphinites at 160 °C

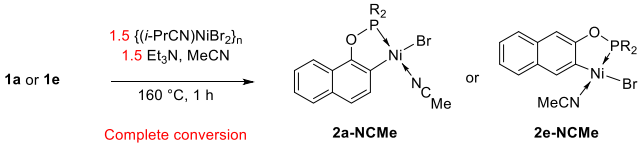

Driving the nickelation of **1a** to completion necessitated a larger excess of the precursor $\{(i\text{-PrCN})NiBr_2\}_n$, because this compound decomposes partially at 160 °C to give Ni black deposition on the walls of the reaction flask and on the stir bar.[17] Thus, using 1.5 equiv of both $\{(i\text{-PrCN})NiBr_2\}_n$ and Et_3N led to complete nickelation of **1a** within 1 h at 160 °C. An even greater acceleration was noted for the much more sluggish nickelation of 2-naphthyl phosphinite **1e**: applying the above reaction conditions (i.e., 50% excess Ni precursor, 160 °C) led to complete conversion to the nickelation product **2e** in 1 h, much faster than the 60 h required for complete nickelation of this substrate at 80 °C (Scheme 9).

Having identified optimal conditions for the high temperature nickelation of **1a** and **1e**, we conducted a few small scale test reactions (ca. 0.2 mmol) to see if the very sluggish nickelation of **1f** (>10 d at 80 °C, Scheme 6) can be accelerated at higher temperatures. Unfortunately, these attempts were unsuccessful as we obtained mostly Ni black and other undesired side-products (Figure S127). For instance, conducting the reaction at 160 °C over 2 h gave a mixture in which the desired cyclonickelated species **2f-NCMe** showed only a minor ^{31}P signal at 192 ppm. Numerous additional signals were also observed, including some in the 50−100 ppm range believed to be phosphinite and phosphine oxides (Ni-bound or free) and an unassigned sharp signal at 123 ppm, in addition to signals around 135 ppm attributed to adducts of the unreacted phosphinite.

On the other hand, lowering the reaction temperature reduced the extent of thermal degradation and gave higher

DOI: 10.1021/acs.organomet.9b00660
Organometallics XXXX, XXX, XXX−XXX

conversions to the target product over shorter reaction times (Scheme 10). For instance, conducting the reaction at 120 °C

Scheme 10. Nickelation of Phosphinite 1f at 160 °C and Protonation of 2f-L in Toluene

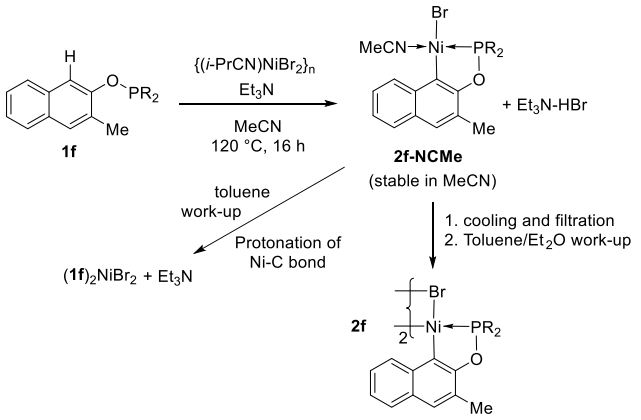

(1.2 equiv each of $\{(i\text{-PrCN})NiBr_2\}_n$ and Et_3N) gave **2f-NCMe** in 43% after 3 h (Figure S135).[18] These results should be compared to ca. 16% yield for the same nickelated product when the reaction is conducted over 7 days at 80 °C. The above encouraging results prompted us to see if conducting mmol scale reactions at 120 °C would allow us to isolate the cyclonickelated MeCN adduct **2f-NCMe** and eventually work it up into its corresponding dimeric complex **2f**. Indeed, heating **1f** with 1.2 equiv of both Et_3N and $\{(i\text{-PrCN})NiBr_2\}_n$ at 120 °C for 16 h gave mostly the desired **2f-NCMe**, as inferred from the observation of a very major peak at 192 ppm assigned to this compound.

An initial attempt to isolate the dimeric species **2f** failed, however, because the workup in toluene led to reprotonation of the nickelated species with $Et_3N{\cdot}HBr$, giving back the non-nickelated complex (Scheme 10). To circumvent this reversal of the nickelation step, the crude reaction mixture was cooled to −35 °C to allow crystallization of unreacted **3f** and of some $Et_3N{\cdot}HBr$. The green supernatant was then evaporated, extracted with toluene, and evaporated to give an orange solid, which was recrystallized from Et_2O to give orange crystals that were identified as **2f**. As will be discussed below, this compound displayed a strong structural distortion.

Lastly, we conducted a few experiments to see if substrate **1d**, which could not be induced to undergo nickelation under the standard reaction conditions at 80 °C, might be nickelated at high temperatures. Unfortunately, the ^{31}P NMR spectrum of the final mixture obtained from the 160 °C reaction of **1d** with $\{(i\text{-PrCN})NiBr_2\}_n$ and Et_3N did not show the anticipated signals for a nickelation product. We found instead a major species at 123 ppm as well as a number of minor signals in the 90−110 and 160−170 ppm regions. Moreover, much Ni black was found deposited on the walls of the reaction vial, and this after only 1 h of reaction. As before, control experiments showed that no degradation of **1d** occurs after 1 h of heating at 160 °C in MeCN, implying that the degradation likely involves the putative nickelated product. Lowering the nickelation temperature to 120 °C led to less thermal degradation, but the makeup of the reaction mixture remained fairly unchanged.

Interception of Unanticipated C−P Functionalized Products. The results discussed in the previous section showed us that high temperatures can have dramatically different impacts on the C−H nickelation of different substrates. With substrates such as **1a** and **1e** that undergo slow C−H nickelation at 80 °C, high temperatures accelerated the cyclonickelation significantly. On the other hand, with a substrate such as **1d** that does not undergo C−H nickelation at 80 °C, high temperatures resulted in a great deal of decomposition. This observation suggested that disrupting the formation of stable cyclonickelated products at high temperatures might open new reactivity pathways. To test this assertion, we set out to conduct the high temperature nickelation of **1a** in the absence of base, which we reasoned would suppress formation of the normal nickelation product **2a-NCMe** and divert the reaction toward alternative pathways.

Thus, heating an acetonitrile solution of 1-naphthyl-phosphinite **1a** and 1.2 equiv of $\{(i\text{-PrCN})NiBr_2\}_n$ at 160 °C over 4 h in the absence of Et_3N gave a red mixture that displayed two major sets of ^{31}P NMR resonances not observed previously, namely: a set of AB doublets at 180 and 30 ppm ($J_{PP} \sim 69$ Hz), and a singlet at 121 ppm. A few other species were also detected, including the non-nickelated phosphinite adduct **3a** represented by a broad signal at ca. 135 ppm. Cooling the mixture to r.t. caused the precipitation of unreacted starting material, **3a**, which was removed by filtration. Cooling the filtrate to −35 °C overnight afforded red crystalline blocks, which were shown via XRD analysis to contain the new compound *cis*-($\kappa^P,\kappa^{P'}$-2-P(*i*-Pr)$_2$-1-naphhtyl-OP(*i*-Pr)$_2$)$NiBr_2$, **4**, shown in Scheme 11.

Scheme 11. C−P Functionalization of 1a

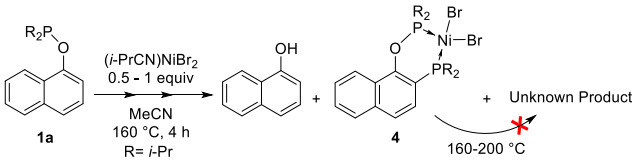

The unanticipated formation of the new phosphinite/phosphine compound **4** can be viewed as the formal insertion of $[i\text{-Pr}_2P]^+$ into the C−Ni bond generated from C−H nickelation of ligand **1a**. It occurred to us that the presence of an excess of substrate might favor this pathway, because transformation of **1a** to **4** requires a 2:1 molar ratio of **1a**:Ni. Indeed, repeating the above reaction with twice as much **1a** as before gave a red mixture for which the ^{31}P NMR spectrum seemed cleaner than the spectrum obtained from the first reaction, even though the reaction was not complete after 4 h. Increasing the reaction temperature to 200 °C resulted in complete consumption of the starting material within 1 h.[19]

Cooling the final reaction mixture overnight to −35 °C yielded a crop of thin needles consisting of elongated plates stuck together. XRD analysis of a crystal obtained from this batch showed it to be poorly diffracting and twinned; nevertheless, the data allowed us to establish that it contained compound **4** and 1/2 molecule of free 1-naphthol (Scheme 11, Figure S182). As will be discussed below, the in situ formation of 1-napthhol in this reaction is significant, because it provides a significant clue for the reaction mechanism.

Another mechanistically relevant observation was that heating a MeCN solution of the cocrystals isolated from this reaction to 160−200 °C showed only the ^{31}P resonances assigned to **4** (two ^{31}P doublets at 180 and 30 ppm), no trace of the unidentified peak at 121 ppm being detected. This implied that the unidentified species is the product of a

DOI: 10.1021/acs.organomet.9b00660
Organometallics XXXX, XXX, XXX−XXX

different side reaction and does not arise from thermal degradation of **4**.

Combining the above clues suggested that the conversion of **1a** to **4** proceeds by the following sequence of steps: (a) cyclonickelation would initially generate HBr and **2a-NCMe**; (b) substitution of MeCN in the latter species by the non nickelated phosphinite **1a** would give the phosphinite adduct **2a-L**;[20] (c) this intermediate would then undergo a rearrangement to initiate the C−P bond forming process; (d) the naphthoxide leaving group generated in this last step would capture the proton produced at the nickelation step (a) to give the naphthol molecule cocrystallized with **4**.

To test the validity of the above postulate, we generated **2a-NCMe** in situ by dissolving the independently prepared dimeric complex **2a** in MeCN, and heated it in the presence of 1 equiv of the phosphinite **1a** at 160 °C for 1 h. Analysis of the final red mixture by ^{31}P NMR showed only a trace of the diagnostic AB doublet for **4**, in addition to broadened signals for unreacted **2a-NCMe** and **1a**, as well as minor peaks in the region of phosphine and phosphinite oxides. This experiment showed that the formation of **4** does not proceed to any appreciable extent from the treatment of **2a-NCMe** with **1a**.

Upon reflection, it occurred to us that the main difference between the reaction depicted in Scheme 11 and the above test is the use of independently prepared **2a-NCMe** in the latter case vs its formation via in situ cyclonickelation in the former case. Given that in situ cyclonickelation generates HBr as a coproduct, we reasoned that this might be an important factor for transformation of **2a-NCMe** into **4**. For instance, the presence of in situ generated HBr might convert the phosphinite **1a** into BrP(*i*-Pr)$_2$, and this might be more reactive for transforming **2a-NCMe** into **4**.

To test the above possibility, we prepared BrP(*i*-Pr)$_2$[9] and heated it with independently prepared **2a-NCMe** (MeCN, 160 °C, 1 h). The ^{31}P NMR spectrum of the resulting red mixture showed complete disappearance of the starting material and formation of the anticipated AB signals of **4** as the major component of the mixture (Figure S146). This result supports the putative mechanism shown in Scheme 12. We speculate

Scheme 12. Postulated Mechanism for Formation of 4

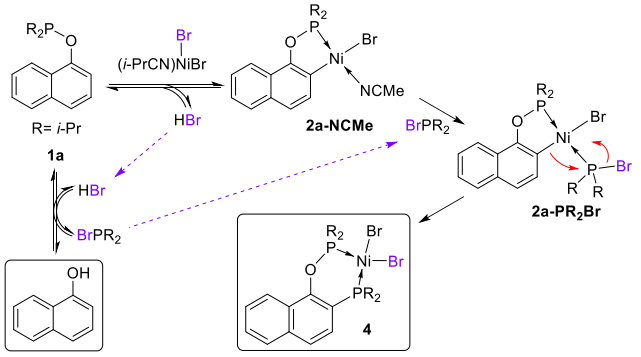

that the C−P bond formation step involves a nucleophilic attack by the Ni-bound aryl moiety on the P nucleus of the coordinated BrP(*i*-Pr)$_2$, but other pathways can also be envisaged. It should be added that we are not aware of a precedent for the formal insertion of a phosphenium fragment into a Ni-aryl bond as shown in Scheme 12, but a closely related inverse of this reactivity has been observed previously. Indeed, a number of reports have documented the extrusion of $[R_2P]^+$ from cationic imidazoliophosphines coordinated to Pd(II) and Ni(II) to generate the corresponding NHC-carbenes.[21]

Having identified complex **4** and proposed a plausible mechanism for its formation from **1a**, we set out to identify the other product observed during this transformation, i.e., the minor species represented by the ^{31}P singlet at 121 ppm. As mentioned above, we concluded that this species does not arise from the thermal degradation of **4**. We posited that it might also be a C−P functionalization product, but one that arises via a competing C−H nickelation at C8. To test this possibility, we examined the analogous reaction of substrate **1d** at 160 °C and in the absence of Et$_3$N, based on the reasoning that the ethyl substituent in **1d** would block C−H nickelation at C2, thereby suppressing the reactivity pathway leading to **4**. Thus, heating a 1:1.2 MeCN mixture of **1d** and {(*i*-PrCN)NiBr$_2$}$_n$ at 160 °C for 1 h gave an emerald green suspension and a Ni mirror on the reactor walls.[22] Filtration of this suspension gave a mixture of Ni black and a mass of light green/yellowish solid, which was identified as {NiBr$_2$(NCMe)$_2$}$_n$. Analysis of the emerald green filtrate by ^{31}P NMR spectroscopy showed a major singlet at 123 ppm, plus very minor resonances at 135, 95, and ca. 45 ppm.

The above filtrate was cooled and filtered to remove more of {NiBr$_2$(NCMe)$_2$}$_n$ in addition to a few deep-red crystals, which were revealed by XRD analysis to be *cis*-(*i*-Pr$_2$PH)$_2$NiBr$_2$.[23] Evaporation of the supernatant gave a green oil, which was washed with toluene and analyzed by NMR (CD$_3$CN, Figure S151). The ^{31}P NMR spectrum of this sample showed the expected singlet at 123 ppm, whereas its ^{1}H NMR spectrum showed two components, the minor one being identified as 2-Et-1-naphthol and the major one displaying the characteristic signals for the P(*i*-Pr)$_2$ moiety and the Et substituent in addition to only 5 resonances in the aromatic region (instead of 6 that would be expected for a monosubstituted naphthol derivative). Adding Et$_2$O to this NMR sample afforded colorless crystals that were identified by XRD analysis as 2-Et-8-(*i*-Pr$_2$P(O))-1-naphthol (compound **5** in Scheme 13), cocrystallized with 1/2 molecule of 2-Et-1-naphthol itself. It should be mentioned that we also obtained crystals for **5·HBr** (Figure S189).

Scheme 13. Tandem C−H Nickelation/C−P Functionalization at C8−H of 1d[a]

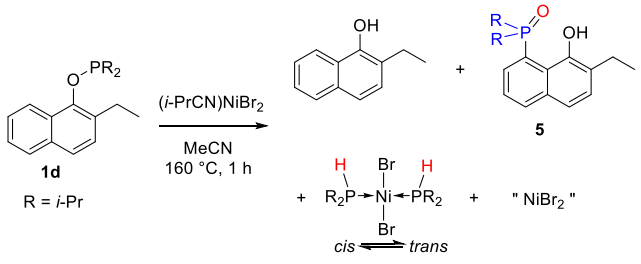

[a]For molecular diagrams of (*i*-Pr$_2$PH)$_2$NiBr$_2$ and **5**·(2-Et-1-naphthol)$_{0.5}$, see Figures S187 and S188.

The question arises whether the ^{31}P resonance at 123 ppm detected for the side-product of the high temperature reaction of **1d** represents the phosphine oxide **5** or its Ni complex. To shed some light on this question, we repeated the reaction of **1d** with {(*i*-PrCN)NiBr$_2$}$_n$ (1:1; MeCN, 160 °C, 1h), added 2 equiv of PPh$_3$ to the crude reaction mixture, and then recorded

DOI: 10.1021/acs.organomet.9b00660
Organometallics XXXX, XXX, XXX−XXX

its ^{31}P NMR spectrum. This showed only the peak at 123 ppm and no new peak for free PPh_3, which implies the in situ formation of the tetrahedral (and NMR-silent) $(PPh_3)_2NiBr_2$ from the reaction of free $NiBr_2$ with added PPh_3. We infer, therefore, that the phosphine oxide **5** generated in this reaction is not Ni-bound. Moreover, solubility tests showed that **5** is soluble in MeCN but insoluble in toluene; the same pattern of solubility was found for the unidentified species generated from the reaction of **1a** (Scheme 11) and represented by a ^{31}P singlet at 121 ppm. The latter has also been analyzed by GC–MS, thus allowing us to identify it as 8-(i-$Pr_2P(O)$)-1-naphthol.

We propose, therefore, that the formation of the phosphine oxides discussed above, **5** from **1d** and the unidentified species in Scheme 11, involves C–H nickelation at C8, followed by the formal insertion of a "$[i\text{-}Pr_2P]^+$" into the C–Ni bond. The 7-membered nickelacycles present in the resulting species would likely be thermally unstable and prone to decomposition. The main aspect that still remains obscure is how the phosphinite moiety at C1 is transformed into $(i\text{-}Pr_2PH)_2NiBr_2$ (Scheme 14).

Scheme 14. Postulated Mechanism for Formation of 5

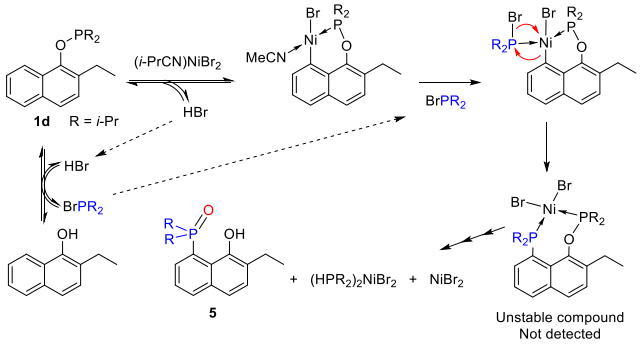

Solid State Structures of Dimers and Complex 4.[24]

The solid state structures of the dimeric complexes **2a**, **2b**, **2c**, and **2e** (Figure 3) share some of the main features found in the structures of the analogous dimeric complexes derived from phenyl phosphinites.[5] Thus, the Ni centers in all dimers adopt a geometry that is very close to square planar, with τ_4 values[14] ranging from 0.05–0.07 for dimers sitting on an inversion center (**2c** and **2e**) and 0.08–0.13 for those not generated by a symmetry operation (**2a** and **2b**). However, the Ni–μ-Br–Ni angle in **2a** was found significantly smaller than the others (85–87° vs <92°), which translates into a noncoplanarity of the two halves of the dimer (Table 1).

Indeed, the hinge angle between the two halves (the dihedral angle Ni1–Br1–Br2–Ni2) was found to be ca. 140° with **2a**, which strongly deviates from the 180° observed in symmetric structures **2c** and **2e**, and from the ca. 177° observed in **2b**. The two Ni centers in **2a** are thus brought closer to each other with a Ni–Ni distance of less than 3.3 Å, shorter than the Ni–Ni distance of 3.4 Å in the planar complexes. These features have already been observed in cyclometalated phenyl phosphinite complexes of Ni[5] and cyclometalated phosphines of Pd;[25] in the case of Ni, this "bent" conformation is thought to be more stable in solution than the planar one observed in crystallized centrosymmetrical complexes.

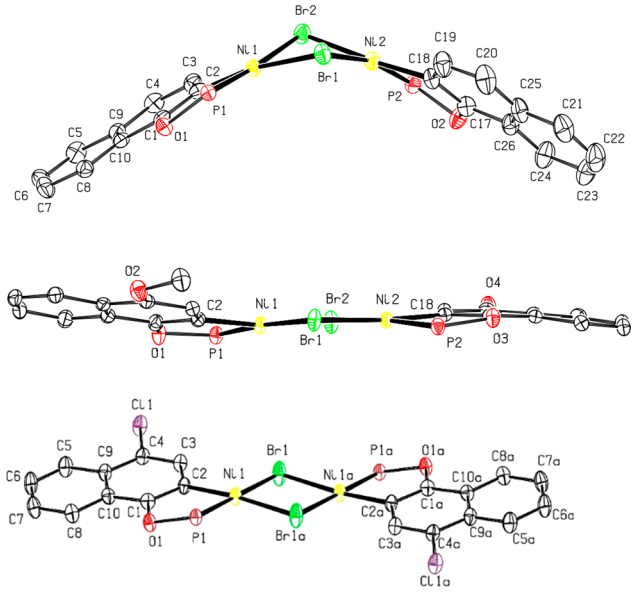

Figure 3. Side views of the molecular diagrams for complexes **2a** (top), **2b** (middle), and **2c** (bottom). Thermal ellipsoids are shown at the 50% probability level; hydrogens and *P*-substituents are omitted for clarity.

The data in Table 1 also show fairly narrow ranges for the bond distances C–Ni (1.908–1.921(2) Å) and P–Ni (2.099(1) – 2.111(1)), and also for the C–Ni–P bite angles (82°–83°); evidently, the different electronic character of the naphthol substituents appears to have little or no impact on these parameters. The Ni–Br bonds also showed a fairly narrow range of distances in complexes **2a**, **2c**, and **2e**: 2.365–2.398 Å over all 14 bonds *trans* or *cis* to the C–Ni bonds. The outlier in this category is complex **2b**, the only "flat" dimer not generated by a symmetry element, which shows greater differences for the Ni–Br distances *trans* or *cis* to Ni–C bond: 2.342 vs 2.413 Å; 2.402 vs 2.375 Å respectively.

One structure that justifies some additional discussion here is that of **2f** (Figure 4), the naphthyl phosphinite adduct of the cyclometalated complex derived from **1f**, because it can help rationalize the C3/C1 regioselectivity observed in the C–H nickelation of 2-naphthyl phosphinite **1e**. The solid state structure of **2f** displays a significantly acute *trans* angle for P–Ni–Br (156°), a tetrahedral distortion with a τ_4 value of 0.22, and a naphthalene ring that bends out of the ideal plane around Ni to give a C10–C1–Ni–Br dihedral of ca. 47° (as opposed to an aromatic plane twisted by less than 10° in similar dimeric compounds).

We believe that the tetrahedral distortion referred to above serves the purpose of minimizing any steric contact of the C8–H moiety of the rigid naphthalene ring with the ligand *cis* to C1–Ni (μ-Br for **2f** and P for **2f-L**). Moreover, it is reasonable to conclude that this steric hindrance would lead to a higher energy barrier for the nickelation of **1e** at C1–H, thus explaining the observed preference for nickelation at C3–H.

Finally, the structure of the bis-phosphine/phosphinite complex **4** is worth discussing because the bidentate ligand creates a 6-membered chelating environment around Ni. Although the P1–Ni1–P2 bite angle of 94° is close to the ideal value, this brings about a significant tetrahedral distortion with a τ_4 of ca. 0.29, and the naphthalene ring is pushed out of the mean plane around Ni by 46° (Figure 5).

DOI: 10.1021/acs.organomet.9b00660
Organometallics XXXX, XXX, XXX–XXX

Table 1. Selected Structural Parameters, Bond Distances (Å), and Bond Angles (°) for Cyclonickelated Dimers

	space group	Ni−C	Ni−P1	*trans*-Ni−Br[a]	*cis*-Ni−Br[a]	C−Ni−P1	Br−Ni−L	τ_4
2a	$Pca2_1$	1.914(5)	2.1050(14)	2.3868(9)	2.3975(9)	81.8	87.0	0.098
		1.908(5)	2.1031(15)	2.3818(10)	2.3810(9)	81.8	87.5	0.126
		1.911(5	2.1006(15)	2.3853(10)	2.3819(9)	82.0	87.2	0.114
		1.917(5)	2.1028(14)	2.3978(9)	2.3854(9)	82.1	86.9	0.116
2b	*Pbca*	1.908(2)	2.1063(7)	2.34241(4)	2.4133(4)	83.1	86.9	0.101
		1.915(2)	2.1105(7)	2.4021(4)	2.3751(5)	82.1	86.4)	0.080
2c	$P\bar{1}$	1.912(4)	2.1036(11)	2.3685(8)	2.3642(7)	82.1	87.4	0.074
		1.914(4)	2.1062(11)	2.3647(7)	2.3714(7)	82.6	87.4	0.054
2e	$P2_1/n$	1.921(2)	2.0992(6)	2.3862(4)	2.390	82.8	86.9	0.052
2f	$P2_1/n$	1.9232(16)	2.0872(5)	2.3880(3)	2.408	80.7	88.3	0.224

[a]*cis* and *trans* positions are relative to the Ni−C bond.

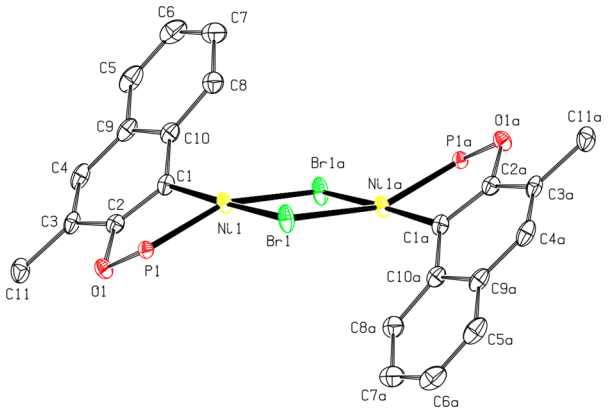

Figure 4. Side view of the molecular diagram for complex **2f**. Thermal ellipsoids are shown at the 50% probability level; hydrogens and *P*-substituents are omitted for clarity.

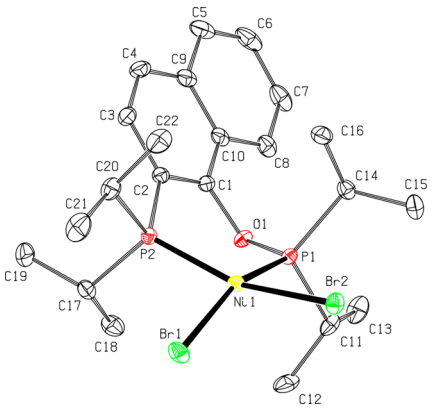

Figure 5. Molecular diagram for complex **4**. Thermal ellipsoids are shown at the 50% probability level; hydrogens are omitted for clarity.

The Ni1−P1 distance of 2.1247(5) Å is longer than in the corresponding *ortho*-nickelated phosphinites, but still much shorter than the Ni-phosphinite distances of ≥ 2.23 Å observed in L_2NiBr_2 complexes featuring non cyclonickelated phosphinites; this is presumably due to the chelate effect in **4**. Similarly, the Ni1−P2 distance of 2.1767(5) Å is longer than P1−Ni1, but still shorter than the corresponding Ni−P distances of ca. 2.23−2.33 Å seen for monodentate $(i\text{-Pr})_2$PPh; it is also comparable to the Ni−P distances in *cis*-(diphosphine)NiX_2 complexes (2.137−2.176 Å). The two *cis* Ni−Br bonds were found to be 2.3390(3) and 2.3405(3) Å, and thus not significantly different; on the other hand, these distances are significantly longer than those in *trans*-(phosphinite)$_2NiBr_2$ complexes characterized throughout this study.

CONCLUSION

This study has established that phosphinites derived from 1- and 2-naphthol undergo C−H nickelation when treated with the Ni^{II} precursor $\{(i\text{-PrCN})NiBr_2\}_n$. When these reactions are conducted in the presence of Et_3N, the cyclonickelated products can be isolated in the form of bromo-bridged dimers or adducts of either acetonitrile or the phosphinite ligand itself. Experimentation allowed us to optimize these reactions as a function of phosphinite:Ni:Et_3N molar ratios, reaction temperature, and also the electronic properties of substituents placed at the *para* position of 1-naphthol. The results of these studies showed that reaction temperature has a great influence on C−H nickelation rates. For instance, the 2-naphthyl phosphinite **1e** is quantitatively converted to the dimeric cyclonickelated complex **2e** in 1 h at 160 °C, whereas the analogous reaction at 80 °C requires 60 h.

Another major issue that was addressed in this study was the regioselectivity of C−H nickelation in our system. Of the two potential C−H sites in 1- and 2-naphthyl phosphinites not bearing substituents in the *ortho* positions, the favored site for cyclonickelation is C2 (not C8) with 1-naphthyl phosphinite and C3 (not C1) in 2-naphthyl phosphinite. It is also important to emphasize that a 2-naphthyl phosphinite bearing a Me substituent at the C3 position can undergo nickelation at the alternative C1−H site at the same temperature (albeit more sluggishly), whereas blocking the favored site in 1-naphthyl phosphinite by an alkyl substituent at the C2 position does not facilitate cyclonickelation at C8.

The observation of exclusive nickelation at the C2 site of 1-naphthyl phosphinites is in contrast to the regioselectivity of 1-naphthyl metalation-functionalization with other metals. With Rh, for instance, these substrates react preferentially at C2, but metalation also occurs to some extent at C8.[7] We speculate that the observed inertness of the C8 site toward nickelation can be attributed to two factors. First, the shorter Ni(II) radius (relative to Rh(III)) likely results in a Ni−C8 distance that would be longer than optimal for initiating the C→Ni interaction and the ensuing deprotonation step.[6] Alternatively (or additionally), the putative 6-membered nickelacycle intermediate that would result from C−H nickelation at C8 might be thermodynamically less stable (especially at high temperatures) relative to the 5-membered metalacyclic transition state that leads to the observed products **2a**−**2c**.

Perhaps the most unexpected result of the present study has been the serendipitous discovery of a tandem C−P

DOI: 10.1021/acs.organomet.9b00660
Organometallics XXXX, XXX, XXX−XXX

functionalization reaction that leads to the "insertion" of a [*i*-Pr_2P]$^+$ or [*i*-$Pr_2P(O)$]$^+$ moiety into the Ni−C site generated by cyclonickelation of the phosphinites derived from 1-naphthol or 2-Et-1-naphthol, respectively. In the first case, the functionalization requires conducting the C−H nickelation at high temperatures (160−200 °C) and in the absence of Et_3N. The available mechanistic information indicates that the C−P bond formation in this case proceeds via a nucleophilic attack by the Ni−C moiety on in situ generated $BrP(i\text{-}Pr)_2$. This C−P functionalization reaction product provides further support for the conclusions we have drawn from our earlier studies, namely: (a) C−H nickelation can take place in the absence of external base, and (b) HBr generated in situ in the C−H nickelation step can leave the coordination sphere of the Ni center and linger in the reaction medium long enough to allow it to react with other species, including H/D exchange with the solvent.

A more complex "insertion"-type C−P functionalization occurs during the high temperature C−H nickelation of the phosphinite derived from 2-Et-1-naphthol. In this case, the "insertion" takes place at C8 and the product is 2-Et-8-(*i*-$Pr_2P(O)$)-1-naphthol, **5**. A related though not identical side-reaction also takes place during the high temperature C−H nickelation of 1-naphthyl phosphinite, but the product of this insertion at C8 is a minor component of the final mixture.

Future investigations will aim to improve our understanding of these interesting functionalization reactions. We will also explore the potential reactivities of the cyclonickelated compounds described herein for oxidation-induced C−heteroatom functionalization reactions. These studies will draw inspiration from recently reported model systems based on NCN-type pincer-Ni^{III} complexes that promote C−N, C−O, and C−halide bond formation reactions.[26]

EXPERIMENTAL SECTION

General Considerations. All manipulations were carried out under a nitrogen atmosphere using standard Schlenk techniques and an inert-atmosphere glovebox. The reactions conducted in acetonitrile at temperatures above its boiling point (120−200 °C) were carried out in a conductively heated, sealed vessel autoclave with a reaction volume of ca. 5 mL (Anton-Paar Monowave 50).[27] The heating program allowed the reaction mixtures to rapidly attain the target temperature and maintain it for the desired reaction time. Solvents were dried by passage over a column of activated alumina, collected under nitrogen, and stored over 3 Å molecular sieves. Triethylamine was dried over CaH_2. Synthesis of the nickel precursor {(*i*-PrCN)$NiBr_2$}$_n$ used throughout this study has been described previously.[28] 1-Naphthol-d_8 was purchased from CDN Isotopes, whereas other reagents were purchased from Sigma-Aldrich or Fisher Scientific and used without further purification.

The NMR spectra were recorded at 500 MHz (^{1}H), 125.72 MHz (^{13}C), and 202.4 MHz (^{31}P). Chemical shift values are reported in ppm (δ) and referenced internally to the residual solvent signals (^{1}H and ^{13}C: 1.94 and 118.26 ppm for CD_3CN; 7.26 and 77.16 for $CDCl_3$; 7.16 and 128.06 for C_6D_6) or externally (^{31}P: H_3PO_4 in D_2O, δ = 0). J coupling values are given in Hz. The NMR spectroscopic data for the dimers correspond to the monomeric $NCCD_3$ adducts in CD_3CN. The elemental analyses were performed by the Laboratoire d'Analyse Élementaire, Département de Chimie, Université de Montreal.

Single crystals of the structurally characterized complexes were grown as follows: by slow evaporation of an Et_2O solution under inert atmosphere for the dimeric complexes **2a**, **2b**, **2c**, **2e** and **2f**; from hot acetonitrile for **2e-NCMe**, **3a**, **3d**, **3f**, **3g**, and **4**; from an acetonitrile solution cooled to −35 °C for (*i*-$Pr_2PH)_2NiBr_2$; from a toluene solution cooled to −35 °C for **3f-L**; from slow diffusion of pentane into an Et_2O solution at −35 °C for **2g**.

Synthesis of the Dimers Derived from Naphthols. To a solution of the desired naphthol (2.00 mmol) in 20 mL dry THF was added 1.10 equiv Et_3N (2.20 mmol, 307 μL), followed by 1.05 equiv $ClP(i\text{-}Pr)_2$ (2.10 mmol, 334 μL); salt precipitation started almost instantaneously. The mixture was stirred at room temperature for 0.5 to 4 h until reaction was complete (monitoring by ^{31}P NMR). The solvent was then removed under vacuum, and the residues were extracted with Et_2O (3 × 15 mL) and evaporated to yield a colorless to pale yellow oil, to which was added 15 mL dry MeCN, 1.2 equiv {(*i*-PrCN)$NiBr_2$}$_n$ (2.40 mmol, 691 mg) and 1.2 equiv Et_3N (2.40 mmol, 335 μL). The brownish-green homogeneous mixture was stirred at 80 °C until the reaction was complete (monitored by the disappearance of the ^{31}P signal for the starting material at ca. 135 ppm). The solvent was then removed under vacuum, and the residues were extracted with toluene through filtration on Celite. The filtrate was evaporated under vacuum, the residues were extracted into a few mL Et_2O (sonication), hexanes added to precipitate the product, followed by filtration and washing with a minimum of hexanes to complete removal of unreacted material/toluene. The solid was dried under vacuum to yield an orange powder. Single crystals were obtained from slow evaporation in Et_2O under N_2.

{(κ^P,κ^C-1-OP(*i*-Pr)$_2$-naphth-2-yl)Ni(μ-Br)}$_2$ (2a). Yield: 587 mg of an orange powder (0.738 mmol, 74%). ^{1}H NMR (500 MHz, 20 °C, CD_3CN) δ 1.37 (dd, 6H, $CH(CH_3)(CH_3)$, $^3J_{HH}$ = 7.0, $^3J_{HP}$ = 14.9), 1.50 (dd, 6H, $CH(CH_3)(CH_3)$, $^3J_{HH}$ = 7.2, $^3J_{HP}$ = 17.6), 2.55 (oct, 2H, $CH(CH_3)_2$, $^3J_{HH} \approx {}^2J_{HP}$ = 7.2), 7.23 (d, 1H, $C4_{Ar}$−*H*, $^3J_{HH}$ = 8.3), 7.33 (dd, 1H, $C3_{Ar}$−*H*, $^3J_{HH}$ = 8.5, $^4J_{HP}$ = 1.3), 7.36−7.40 (m, 2H, $C6_{Ar}$−*H* and $C7_{Ar}$−*H*), 7.72−7.78 (m, 1H, $C5_{Ar}$−*H*), 7.87−7.92 (m, 1H, $C8_{Ar}$−*H*). ^{13}C{^{1}H} NMR (125.7 MHz, 20 °C, CD_3CN) δ 16.82 (d, 2C, $CH(CH_3)(CH_3)$, $^2J_{CP}$ = 2.0), 18.43 (d, 2C, $CH(CH_3)(CH_3)$, $^2J_{CP}$ = 2.8), 29.14 (d, 2C, $CH(CH_3)(CH_3)$, $^1J_{CP}$ = 28.8), 120.28 (d, 1C, $C4_{Ar}$−H, $^4J_{CP}$ = 1.6), 121.54 (d, 1C, C_{quat}, $^4J_{CP}$ = 12.5), 122.50 (d, 1C, $C8_{Ar}$−H), 125.69 (s, 2C, $C6_{Ar}$−H and $C7_{Ar}$−H), 127.70 (s, 1C, $C5_{Ar}$−H), 127.68 (d, 1C, $C2_{Ar}$−Ni, $^2J_{CP}$ = 34.7), 134.03 (s, 1C, C_{quat}), 134.87 (d, 1C, $C3_{Ar}$−H, $^3J_{CP}$ = 2.7), 161.95 (d, 1C, $C1_{Ar}$−OP, $^3J_{CP}$ = 12.6). ^{31}P{^{1}H} NMR (202.4 MHz, 20 °C, $CDCl_3$) δ 195.77. Anal. Calc. for $C_{32}H_{40}Br_2Ni_2O_2P_2$: C, 48.30; H, 5.07. Found: C, 47.73; H, 5.00; N, 0.06.

{(κ^P,κ^C-4-MeO-1-OP(*i*-Pr)$_2$-naphth-2-yl)Ni(μ-Br)}$_2$ (2b). Yield: 721 mg of an orange powder (0.842 mmol, 84%). ^{1}H NMR (500 MHz, 20 °C, CD_3CN) δ 1.36 (dd, 6H, $CH(CH_3)(CH_3)$, $^3J_{HH}$ = 7.0, $^3J_{HP}$ = 14.9), 1.49 (dd, 6H, $CH(CH_3)(CH_3)$, $^3J_{HH}$ = 7.2, $^3J_{HP}$ = 17.6), 2.52 (oct, 2H, $CH(CH_3)_2$, $^3J_{HH} \approx {}^2J_{HP}$ = 7.2), 3.93 (s, 3H, $C4_{Ar}$−OCH_3), 6.69 (s, 1H, $C3_{Ar}$−*H*), 7.35−7.45 (m, 2H, $C6_{Ar}$−*H* and $C7_{Ar}$−*H*, $^3J_{HH} \approx$ 7.0, $^4J_{HH} \approx$ 1.6), 7.81 (dm, 1H, $C8_{Ar}$−*H*, $^3J_{HH}$ = 7.6), 8.03 (dm, 1H, $C5_{Ar}$−*H*, $^3J_{HH}$ = 7.6). ^{13}C{^{1}H} NMR (125.7 MHz, 20 °C, CD_3CN) δ 17.05 (d, 2C, $CH(CH_3)(CH_3)$, $^2J_{CP}$ = 2.0), 18.69 (d, 2C, $CH(CH_3)(CH_3)$, $^2J_{CP}$ = 2.7), 29.36 (d, 2C, $CH(CH_3)(CH_3)$, $^1J_{CP}$ = 28.9), 56.04 (s, 1C, $C4_{Ar}$−OCH_3), 113.30 (d, 1C, $C3_{Ar}$−H, $^3J_{CP}$ = 3.0), 121.89 (d, 1C, C_{quat}, $^4J_{CP}$ = 12.7), 122.38 (s, 1C, $C5_{Ar}$−H), 122.72 (s, 1C, $C8_{Ar}$−H), 125.18 (s, 1C, $C6_{Ar}$−H), 125.69 (s, 1C, C_{quat}), 126.50 (s, 1C, $C7_{Ar}$−H), 124.18 (d, 1C, $C2_{Ar}$−Ni, $^2J_{CP}$ = 35.2), 148.71 (d, 1C, $C4_{Ar}$−OCH_3, $^4J_{CP}$ = 2.6), 156.38 (d, 1C, $C1_{Ar}$−OP, $^3J_{CP}$ = 12.3). ^{31}P{^{1}H} NMR (202.4 MHz, 20 °C, $CDCl_3$) δ 193.60. Anal. Calc. for $C_{34}H_{44}Br_2Ni_2O_4P_2$: C, 47.71; H, 5.18. Found: C, 47.19; H, 5.18; N, 0.12.

{(κ^P,κ^C-4-Cl-1-OP(*i*-Pr)$_2$-naphth-2-yl)Ni(μ-Br)}$_2$ (2c). Yield: 633 mg of an orange powder (0.767 mmol, 77%). ^{1}H NMR (500 MHz, 20 °C, CD_3CN) δ 1.37 (dd, 6H, $CH(CH_3)(CH_3)$, $^3J_{HH}$ = 7.0, $^3J_{HP}$ = 15.1), 1.50 (dd, 6H, $CH(CH_3)(CH_3)$, $^3J_{HH}$ = 7.2, $^3J_{HP}$ = 17.8), 2.56 (oct, 2H, $CH(CH_3)_2$, $^3J_{HH} \approx {}^2J_{HP}$ = 7.2), 7.36 (d, 1H, $C3_{Ar}$−*H*, $^4J_{HH}$ = 0.9), 7.47 (ddd, 1H, $C7_{Ar}$−*H*, $^3J_{HH}$ = 8.3, $^3J_{HH'}$ = 7.6, $^4J_{HH}$ = 1.4), 7.53 (tm, 1H, $C6_{Ar}$−*H*, $^3J_{HH}$ = 8.2, $^3J_{HH'}$ = 7.6, $^4J_{HH}$ = 1.4), 7.94 (dm, 1H, $C8_{Ar}$−*H*, $^3J_{HH}$ = 8.4), 8.07 (dm, 1H, $C5_{Ar}$−*H*, $^3J_{HH}$ = 8.4). ^{13}C{^{1}H} NMR (125.7 MHz, 20 °C, CD_3CN) δ 17.15 (d, 2C, $CH(CH_3)(CH_3)$, $^2J_{CP}$ = 2.2), 18.74 (d, 2C, $CH(CH_3)(CH_3)$, $^2J_{CP}$ = 2.6), 29.64 (d, 2C, $CH(CH_3)(CH_3)$, $^1J_{CP}$ = 28.8), 122.54 (d, 1C, C_{quat}

DOI: 10.1021/acs.organomet.9b00660
Organometallics XXXX, XXX, XXX−XXX

or $C4_{Ar}$–Cl, $^4J_{CP}$ = 3.1), 122.66 (d, 1C, C_{quat}, $^4J_{CP}$ = 12.2), 123.70 (s, 1C, $C8_{Ar}$–H), 124.73 (s, 1C, $C5_{Ar}$–H), 127.01 (s, 1C, $C7_{Ar}$–H), 127.28 (s, 1C, $C6_{Ar}$–H), 128.48 (d, 1C, $C2_{Ar}$–Ni, $^2J_{CP}$ = 33.7), 130.71 (s, 1C, C_{quat} or $C4_{Ar}$–Cl), 135.31 (d, 1C, $C3_{Ar}$–H, $^3J_{CP}$ = 2.5), 161.66 (d, 1C, $C1_{Ar}$–OP, $^3J_{CP}$ = 12.5). $^{31}P\{^1H\}$ NMR (202.4 MHz, 20 °C, $CDCl_3$) δ 196.48. Anal. Calc. for $C_{32}H_{38}Br_2Cl_2Ni_2O_2P_2$: C, 44.45; H, 4.43. Found: C, 44.57; H, 4.49.

{(κ^P,κ^C-2-OP(*i*-Pr)$_2$-naphth-3-yl)Ni(μ-Br)}$_2$ (2e). This compound required a modified workup procedure for optimal yields. After evaporation of the crude reaction mixture, 25 mL toluene was added, the mixture stirred at 80 °C for 30 min, followed by filtration (while hot), evaporation, and washing of the solids with Et_2O and hexanes. Yield: 431 mg of an orange powder (0.542 mmol, 54%). The ^1H NMR of the final powder showed that it still contained toluene (ca. 2–5% w/w). Even after extended drying in vacuo at 80 °C, trituration in hexanes, and trituration in Et_2O or Et_2O:CH_2Cl_2 1:1, traces of toluene were still found, although it decreased to ca. 1% w/w (5 mol % vs. Ni). The elemental analysis of this solid showed fair purity. Conversion into the MeCN adduct removed all toluene and resulted in higher NMR purity. ^1H NMR (500 MHz, 20 °C, CD_3CN) δ 1.33 (dd, 6H, CH(CH_3)(CH_3), $^3J_{HH}$ = 7.0, $^3J_{HP}$ = 15.0), 1.48 (dd, 6H, CH(CH_3)(CH_3), $^3J_{HH}$ = 7.2, $^3J_{HP}$ = 17.6), 2.50 (oct, 2H, $CH(CH_3)_2$, $^3J_{HH} \approx {}^2J_{HP}$ = 7.1), 7.01 (s, 1H, $C1_{Ar}$–H), 7.25 (ddd, 1H, $C6_{Ar}$–H, $^3J_{HH}$ = 8.1, $^3J_{HH'}$ = 6.8, $^4J_{HH}$ = 1.3), 7.32 (ddd, 1H, $C7_{Ar}$–H, $^3J_{HH}$ = 8.1, $^3J_{HH'}$ = 6.8, $^4J_{HH}$ = 1.3), 7.61 (d, 1H, $C8_{Ar}$–H, $^3J_{HH}$ = 8.1), 7.66 (s, 1H, $C4_{Ar}$–H), 7.71 (d, 1H, $C1_{Ar}$–H, $^3J_{HH}$ = 8.1). $^{13}C\{^1H\}$ NMR (125.7 MHz, 20 °C, $CDCl_3$) δ 17.18 (d, 2C, CH(CH_3)(CH_3), $^2J_{CP}$ = 2.0), 18.79 (d, 2C, CH(CH_3)(CH_3), $^2J_{CP}$ = 2.7), 29.54 (d, 2C, $CH(CH_3)(CH_3)$, $^1J_{CP}$ = 29.2), 104.98 (d, 1C, $C1_{Ar}$–H, $^4J_{CP}$ = 13.1), 124.18 (s, 1C, $C6_{Ar}$–H), 126.14 (s, 1C, $C7_{Ar}$–H), 127.03 (s, 1C, $C8_{Ar}$–H), 127.73 (s, 1C, $C5_{Ar}$–H), 130.36 (d, 1C, C_{quat}, $^4J_{CP}$ = 2.1), 134.60 (s, 1C, C_{quat}), 138.10 (d, 1C, $C3_{Ar}$–Ni, $^2J_{CP}$ = 36.0), 138.99 (d, 1C, $C4_{Ar}$–H, $^3J_{CP}$ = 2.7), 166.62 (d, 1C, $C1_{Ar}$–OP, $^3J_{CP}$ = 12.1). $^{31}P\{^1H\}$ NMR (202.4 MHz, 20 °C, $CDCl_3$) δ 197.33. Anal. Calc. for $C_{32}H_{40}Br_2Ni_2O_2P_2$: C, 48.30; H, 5.07. Found: C, 48.25; H, 5.21.

{(κ^P,κ^C-3-Me-2-OP(*i*-Pr)$_2$-naphth-1-yl)Ni(μ-Br)}$_2$ (2f). To a solution of 274 mg 3-Me-2-naphthyl-OP(*i*-Pr)$_2$ (1.00 mmol) in 5 mL MeCN were added 345 mg {(*i*-PrCN)$NiBr_2$}$_n$ (1.20 mmol, 1.2 equiv) and 167 μL Et_3N (1.20 mmol, 1.2 equiv). The resulting dark greenish solution that contained a red precipitate of **3f** was heated at 120 °C for 16 h in the Monowave 50. The crude mixture was cooled at −35 °C overnight resulting in crystallization of unreacted **3f** and Et_3N·HBr. The green supernatant was evaporated, extracted with toluene, and the volatiles removed under vacuum at 60 °C. The orange residues were treated with 3 mL Et_2O and filtered, and then the dark orange filtrate cooled at −35 °C overnight to give some orange precipitate. These were removed manually and dried under vacuum to allow NMR characterization, which showed some impurities. Elemental analysis was not performed on this sample. ^1H NMR (500 MHz, 20 °C, CD_3CN) δ 1.24 (dd, 6H, CH(CH_3)-(CH_3), $^3J_{HH}$ = 7.0, $^3J_{HP}$ = 14.7), 1.48 (dd, 6H, CH(CH_3)(CH_3), $^3J_{HH}$ = 7.2, $^3J_{HP}$ = 17.7), 2.29 (d, 3H, Ar–CH_3, $^6J_{HH}$ = 0.7), 2.44 (oct, 2H, $CH(CH_3)_2$, $^3J_{HH} \approx {}^2J_{HP}$ = 7.2), 7.21 (ddd, 1H, $C6_{Ar}$–H, $^3J_{HH}$ = 8.0, $^3J_{HH'}$ = 6.8, $^4J_{HH}$ = 1.2), 7.28 (s, overlapping with δ 7.29, 1H, $C4_{Ar}$–H), 7.29 (ddd, overlapping with δ 7.28, $C7_{Ar}$–H, 1H, $^3J_{HH}$ = 8.3, $^3J_{HH'}$ = 6.8, $^4J_{HH}$ = 1.4), 7.57 (d, 1H, $C5_{Ar}$–H, $^3J_{HH}$ = 8.3), 8.19 (d, 1H, $C8_{Ar}$–H, $^3J_{HH}$ = 8.6). $^{13}C\{^1H\}$ NMR (125.7 MHz, 20 °C, $CDCl_3$) δ 17.22 (d, 2C, CH(CH_3)(CH_3), $^2J_{CP}$ = 2.5), 17.60 (s, 1C, Ar-CH_3), 18.76 (d, 2C, CH(CH_3)(CH_3), $^2J_{CP}$ = 2.8), 29.71 (d, 2C, $CH(CH_3)(CH_3)$, $^1J_{CP}$ = 27.5), 123.22 (d, 1C, $C3_{Ar}$–Me, $^4J_{CP}$ = 11.4), 123.65 (s, 1C, $C6_{Ar}$–H), 124.36 (s, 1C, $C7_{Ar}$–H), 127.65 (d, 1C, $C1_{Ar}$–Ni, $^2J_{CP}$ = 36.6), 128.29 (s, 1C, $C4_{Ar}$–H), 128.32 (s, 1C, $C5_{Ar}$–H), 130.09 (s, 1C, $C8_{Ar}$–H), 131.85 (s, 1C, C_{quat}), 141.09 (d, 1C, C_{quat}, $^3J_{CP}$ = 4.1), 161.65 (d, 1C, $C2_{Ar}$–OP, $^3J_{CP}$ = 10.1). $^{31}P\{^1H\}$ NMR (202.4 MHz, 20 °C, $CDCl_3$) δ 189.85.

(κ^P,κ^C-2-OP(*i*-Pr)$_2$-naphth-3-yl)NiBr(NCMe) (1e-NCMe). *Method A.* 200 mg (250 μmol) of **1e** containing ca. 2–5% w/w residual toluene were dissolved in a minimum amount of MeCN at 80 °C (ca. 12 mL). The resulting yellow solution was slowly cooled down to room temperature, kept in a fridge at −10 °C for 4 h to induce gradual crystallization, and subsequently kept at −35 °C overnight. The resulting yellow crystals were isolated and washed with cold MeCN (2 × 2.5 mL) and dried under vacuum. Yield: 168 mg of yellow crystals (383 μmol, 77%).

Method B. 200 mg (250 μmol) of **1e** containing ca. 2–5% w/w residual toluene were suspended in 10 mL Et_2O. Addition of 130 μL MeCN (2.5 mmol, 10 equiv) turned the orange suspension yellow. The mixture was stirred at room temperature for 30 min and the residues were isolated by cannula filtration, washed with 2 × 5 mL Et_2O, and dried under vacuum. Yield: 174 mg of yellow microcrystalline material (396 μmol, 79%). Anal. Calc. for $C_{18}H_{23}BrNiOP$: C, 49.25; H, 5.28; N, 3.19. Found: C, 49.13; H, 5.44; N, 3.15.

(κ^P,$\kappa^{C\alpha}$,$\kappa^{C\gamma}$-2-CH_2=CH—CH-1-naphtyl-OP(*i*-Pr)$_2$)NiBr (2g). To a solution of 600 mg **1g** (2.00 mmol) in 10 mL acetonitrile were added 575 mg {(*i*-PrCN)$NiBr_2$}$_n$ (2.00 mmol, 1.00 equiv) and 558 μL Et3N (4.00 mmol, 2.00 equiv), and the green mixture was stirred overnight at room temperature The resulting red mixture was evaporated, the residues were redissolved in 6 mL THF, and 10 mL hexanes added to induce precipitation. Filtration and evaporation gave residues, which were treated with 10 mL Et_2O, filtered and evaporated. The resulting residues were dissolved in 2 mL Et_2O, diluted with 2 mL pentane, filtered, and kept at −35 °C overnight. The mixture of orange crystals and other precipitate was evaporated, washed with cold pentane (2 × 2 mL), and dried under vacuum. NMR characterization showed some impurities. Elemental analysis was not performed on this sample. ^1H NMR (500 MHz, 20 °C, CD_3CN) δ 0.88 (dd, 3H, P[CH(CH_3)(CH_3)][CH(CH_3)(CH_3)], $^3J_{HH}$ = 7.1, $^3J_{HP}$ = 13.6), 0.99 (dd, 3H, P[CH(CH_3)(CH_3)][CH-(CH_3)(CH_3)], $^3J_{HH}$ = 7.2, $^3J_{HP}$ = 17.1), 1.24 (dd, 3H, P[CH(CH_3)-(CH_3)][CH(CH_3)(CH_3)], $^3J_{HH}$ = 7.0, $^3J_{HP}$ = 14.7), 1.55 (dd, 3H, P[CH(CH_3)(CH_3)][CH(CH_3)(CH_3)], $^3J_{HH}$ = 7.2, $^3J_{HP}$ = 17.4), 2.32 (hept, 1H, P[$CH(CH_3)_2$][$CH(CH_3)_2$], $^3J_{HH}$ = 7.1), 2.47 (oct, 1H, P[$CH(CH_3)_2$][$CH(CH_3)_2$], $^3J_{HH} \approx {}^2J_{HP}$ = 7.7), 3.16–3.26 (m, 2H, Ar–$C_\alpha H$(Ni) and Ar–C_αH(Ni)-C_βH = C(*Ha*)(Hb) *cis* to $C_\beta H$), 4.36 (dd, 1H, Ar–C_αH(Ni)-C_βH = C(Ha)(*Hb*) *trans* to $C_\beta H$), $^3J_{HH}$ = 7.2, $^2J_{HH'}$ = 4.3), 4.95 (ddd, 1H, Ar–C_αH(Ni)-$C_\beta H$=CH_2), 7.13 (d, 1H, $C3_{Ar}$–H, $^3J_{HH}$ = 8.4), 7.22–7.28 (m, 2H, $C4_{Ar}$–H and $C6_{Ar}$–H), 7.32 (t, 1H, $C7_{Ar}$–H, $^3J_{HH}$ = 7.4), 7.59 (d, 1H, $C5_{Ar}$–H, $^3J_{HH}$ = 8.1), 8.19 (d, 1H, $C4_{Ar}$–H, $^3J_{HH}$ = 8.3). $^{13}C\{^1H\}$ NMR (125.7 MHz, 20 °C, $CDCl_3$) δ 15.72 (d, 1C, P[CH(CH_3)(CH_3)][CH(CH_3)(CH_3)], $^2J_{CP}$ = 1.8), 17.72 (s, 1C, P[CH(CH_3)(CH_3)][CH(CH_3)(CH_3)]), 17.99 (d, 1C, P[CH(CH_3)(CH_3)][CH(CH_3)(CH_3)], $^2J_{CP}$ = 3.6), 18.10 (d, 1C, P[CH(CH_3)(CH_3)][CH(CH_3)(CH_3)], $^2J_{CP}$ = 6.3), 29.48 (d, 1C, P[$CH(CH_3)_2$][$CH(CH_3)_2$], $^1J_{CP}$ = 26.6), 30.41 (d, 1C, P[CH-(CH_3)$_2$][$CH(CH_3)_2$], $^1J_{CP}$ = 15.9), 59.07 (d, 1C, Ar-C_αH(Ni), $^2J_{CP}$ = 5.5), 77.48 (d, 1C, Ar–C_αH(Ni)-C_βH = CH_2, $^2J_{CP}$ = 20.8), 110.92 (d, 1C, Ar–C_αH(Ni)-C_βH = CH_2, $^3J_{CP}$ = 2.5), 120.62 (d, 1C, $C2_{Ar}$–C_αH(Ni), $^3J_{CP}$ = 6.5), 122.23 (s, 1C, $C8_{Ar}$–H), 122.61 (s, 1C, $C4_{Ar}$–H), 126.03 (d, 1C, C_{quat}, $^5J_{CP}$ = 2.9), 126.61 (s, 2C, $C6_{Ar}$–H and $C7_{Ar}$–H), 126.92 (s, 1C, $C3_{Ar}$–H), 128.27 (s, 1C, C5Ar–H, hidden under the peak for C_6D_6), 134.46 (s, 1C, C_{quat}), 151.41 (s, 1C, $C1_{Ar}$–OP). $^{31}P\{^1H\}$ NMR (202.4 MHz, 20 °C, $CDCl_3$) δ 199.72.

Synthesis of Bis-phosphinite-$NiBr_2$ Complexes 3. To a solution of 2.00 mmol of the desired naphthyl phosphinite in 15 mL CH_2Cl_2 was added 403 mg of {(*i*-PrCN)$NiBr_2$}$_n$ (1.40 mmol, 0.7 equiv). The resulting dark red mixture was stirred at room temperature for 30 min. The excess $NiBr_2$ was separated by cannula filtration and the residues extracted with an extra 2 × 15 mL CH_2Cl_2. The combined extracts were evaporated to give orange to red brownish powders that were crystallized from hot MeCN, cooled to room temperature first and then to −10 °C for 3–4 h, and finally placed overnight in a freezer at −35 °C. The resulting dark red crystals were washed with cold MeCN (3 × 5–10 mL), and dried under vacuum. Their purity was established by elemental analysis, whereas ^{31}P and ^1H NMR spectra in $CDCl_3$ suggested they exist as 2 isomers in solution in a ca. 1:9 ratio; we infer that the centrosymmetric structure is the major isomer while the minor one is a C2-symmetric structure or else the cis isomer. For instance, in compound **3f**, both isomers have also been detected in the solid state

DOI: 10.1021/acs.organomet.9b00660
Organometallics XXXX, XXX, XXX–XXX

^{31}P NMR (see Figure S103) at δ 137.10 (major) and 132.45 ppm (minor). In the case of deuterated ligands, the complexes were used as powders in H/D scrambling experiments without crystallization.

***trans*-{1-Naphthyl-OP(*i*-Pr)$_2$}$_2$NiBr$_2$·CH$_3$CN (3a·CH$_3$CN).** This complex cocrystallized with 1 molecule of MeCN per nickel center, yielding 618 mg of dark red crystals (0.79 mmol, 79%). ^{1}H NMR (500 MHz, 20 °C, $CDCl_3$) δ 1.48 (m, 6H, CH(CH_3)(CH$_3$), $^3J_{HH}$ = 6.3), 1.59 (3, 6H, CH(CH$_3$)(CH_3), $^3J_{HH}$ = 6.3), 2.1.99(br s, 1.5H, CH_3CN), 2.84 (hept, 2H, CH(CH$_3$)(CH$_3$), $^3J_{HH}$ = 7.0, minor), 2.92 (hept, 2H, CH(CH$_3$)(CH$_3$), $^3J_{HH}$ = 7.2, major), 7.40−7.48 (m, 2H, C6$_{Ar}$−H and C7$_{Ar}$−H, $^3J_{HH} \approx$ 6.9), 7.50 (t, 1H, C3$_{Ar}$−H, $^3J_{HH}$ = 7.9), 7.59 (d, 1H, C4$_{Ar}$−H, $^3J_{HH}$ = 8.2), 7.81 (d, 1H, C5$_{Ar}$−H, $^3J_{HH}$ = 7.2), 8.10 (d, 1H, C8$_{Ar}$−H, $^3J_{HH}$ = 7.5), 8.42 (d, 1H, C2$_{Ar}$−H, $^3J_{HH}$ = 7.5, major), 8.46 (d, 1H, C2$_{Ar}$−H, $^3J_{HH}$ = 7.6, minor). ^{13}C{^{1}H} NMR (125.7 MHz, 20 °C, $CDCl_3$) δ 2.06 (s, 0.5C, CH_3CN), 18.19 (s, 2C, CH(CH_3)(CH$_3$), minor), 18.48 (s, 2C, CH(CH$_3$)(CH$_3$), major), 19.26 (s, 2C, CH(CH$_3$)(CH$_3$), minor), 19.77 (s, 2C, CH(CH$_3$)-(CH_3), major), 28.91 (s, 2C, CH(CH$_3$)(CH$_3$), minor), 29.98 (s, 2C, CH(CH$_3$)(CH$_3$), major), 113.78 (s, 1C, C2$_{Ar}$−H, minor), 113.95 (s, 1C, C2$_{Ar}$−H, major), 116.53 (s, 1C, CH_3CN), 122.16 (s, 1C, C8$_{Ar}$−H), 122.59 (s, 1C, C4$_{Ar}$−H), 125.11 (s, 1C, C3$_{Ar}$−H, major), 125.3 (s, 1C, C3$_{Ar}$−H, minor), 125.76 (s, 1C, C7$_{Ar}$−H), 126.51 (s, 1C, C6$_{Ar}$−H), 126.60 (s, 1C, C$_{quat}$), 127.78 (s, 1C, C5$_{Ar}$−H), 134.79 (s, 1C, C$_{quat}$), 150.84 (s, 1C, C1$_{Ar}$−OP). ^{31}P{^{1}H} NMR (202.4 MHz, 20 °C, $CDCl_3$) δ 130.37 (s, 1P, minor), 135.65 (s, 1P, major). Anal. Calc. for $C_{34}H_{45}Br_2NNiO_2P_2$: C, 52.34; H, 5.81; N, 1.80. Found: C, 52.64; H, 5.97; N, 1.75.

***trans*-{2-Et-1-naphthyl-OP(*i*-Pr)$_2$}$_2$NiBr$_2$ (3d).** Yield: 439 mg of dark red crystals (0.55 mmol, 55%). ^{1}H NMR (500 MHz, 20 °C, $CDCl_3$) δ 1.08 (m, 6H, CH(CH_3)(CH$_3$), $^3J_{HH}$ = 8.0), 1.21 (t, 3H, Ar−CH$_2$CH_3, $^3J_{HH}$ = 7.6), 1.33 (m, 6H, CH(CH$_3$)(CH_3), $^3J_{HH}$ = 6.6), 2.91 (q, 2H, Ar−CH_2CH$_3$, $^3J_{HH}$ = 7.6), 3.04 (m, 2H, CH(CH$_3$)(CH$_3$), J = 7.0, minor), 3.19 (m, 2H, CH(CH$_3$)(CH$_3$), J = 6.7, major), 7.27 (d, 1H, C3$_{Ar}$−H, $^3J_{HH}$ = 8.5), 7.43 (t, 1H, C6$_{Ar}$−H, $^3J_{HH}$ = 7.4), 7.53 (t, 1H, C7$_{Ar}$−H, $^3J_{HH}$ = 7.6), 7.56 (d, 1H, C4$_{Ar}$−H, $^3J_{HH}$ = 8.5), 7.79 (d, 1H, C5$_{Ar}$−H, $^3J_{HH}$ = 8.1), 8.33 (d, 1H, C8$_{Ar}$−H, $^3J_{HH}$ = 8.3). ^{13}C{^{1}H} NMR (125.7 MHz, 20 °C, $CDCl_3$) δ 14.76 (s, 1C, Ar−CH$_2$CH$_3$), 17.59 (s, 2C, CH(CH$_3$)(CH$_3$), minor), 17.74 (s, 2C, CH(CH_3)(CH$_3$), major), 17.98 (s, 2C, CH(CH$_3$)(CH_3)), 24.54 (s, 1C, Ar-CH_2CH$_3$, minor), 25.67 (s, 1C, Ar-CH_2CH$_3$, major), 29.97 (m, 2C, CH(CH$_3$)(CH$_3$), minor), 31.34 (vt/pt, 2C, CH(CH$_3$)(CH$_3$), $^1J_{CP}$ = 10.3,major), 123.44 (s, 1C, C8$_{Ar}$−H), 123.91 (s, 1C, C4$_{Ar}$−H), 125.42 (s, 1C, C6$_{Ar}$−H), 126.18 (s, 1C, C7$_{Ar}$−H), 127.36 (s, 1C, C3$_{Ar}$−H), 127.84 (s, 1C, C$_{quat}$), 127.92 (s, 1C, C5$_{Ar}$−H), 131.29 (s, 1C, C$_{quat}$), 133.78 (s, 1C, C$_{quat}$), 149.16 (s, 1C, C1$_{Ar}$−OP). ^{31}P{^{1}H} NMR (202.4 MHz, 20 °C, $CDCl_3$) δ 131.50 (s, 1P, minor), 136.10 (s, 1P, major). Anal. Calc. for $C_{36}H_{50}Br_2NiO_2P_2$: C, 54.37; H, 6.34. Found: C, 54.58; H, 6.67; N, 0.05.

***trans*-{3-Me-2-naphthyl-OP(*i*-Pr)$_2$}$_2$NiBr$_2$ (3f).** Yield: 465 mg of dark red crystals (0.61 mmol, 61%). ^{1}H NMR (500 MHz, 20 °C, $CDCl_3$) δ 1.35 (m, 6H, CH(CH_3)(CH$_3$), $^3J_{HH}$ = 6.8), 1.52 (m, 6H, CH(CH$_3$)(CH_3), $^3J_{HP}$ = 6.8), 2.34 (s, 3H, Ar−CH_3), 2.76 (hept, 2H, CH(CH$_3$)(CH$_3$), $^3J_{HH}$ = 7.0, minor), 2.84 (hept, 2H, CH(CH$_3$)-(CH$_3$), $^3J_{HH}$ = 7.2, major), 7.33−7.42 (m, 2H, C6$_{Ar}$−H and C7$_{Ar}$−H, $^3J_{HH} \approx$ 7.8, $^4J_{HH} \approx$ 1.9), 7.57 (s, 1H, C4$_{Ar}$−H), 7.72 (d, 1H, C5$_{Ar}$−H, $^3J_{HH}$ = 8.0), 7.75 (d, 1H, C8$_{Ar}$−H, $^3J_{HH}$ = 8.1), 8.51 (s, 1H, C1$_{Ar}$−H,), major), 8.55 (s, 1H, C1$_{Ar}$−H,), minor). ^{13}C{^{1}H} NMR (125.7 MHz, 20 °C, $CDCl_3$) δ 17.58 (s, 1C, Ar-CH$_3$), 18.01 (s, 2C, CH(CH_3)-(CH$_3$), minor), 18.28 (s, 2C, CH(CH_3)(CH$_3$), major), 19.12 (s, 2C, CH(CH$_3$)(CH$_3$), minor), 19.67 (s, 2C, CH(CH$_3$)(CH$_3$), major), 28.56 (s, 2C, CH(CH$_3$)(CH$_3$), minor), 29.59 (s, 2C, CH(CH$_3$)-(CH$_3$), major), 114.43 (s, 1C, C1$_{Ar}$−H), 124.43 (s, 1C, C6$_{Ar}$−H or C7$_{Ar}$−H), 125.55 (s, 1C, C6$_{Ar}$−H or C7$_{Ar}$−H), 126.94 (s, 1C, C8$_{Ar}$−H), 127.05 (s, 1C, C5$_{Ar}$−H), 129.10 (s, 1C, C4$_{Ar}$−H), 129.60 (s, 1C, C$_{quat}$), 130.14 (s, 1C, C$_{quat}$), 132.74 (s, 1C, C$_{quat}$), 152.35 (s, 1C, C2$_{Ar}$−OP). ^{31}P{^{1}H} NMR (202.4 MHz, 20 °C, $CDCl_3$) δ 129.30 (s, 1P, minor), 134.55 (s, 1P, major). Anal. Calc. for $C_{34}H_{46}Br_2NiO_2P_2$: C, 53.23; H, 6.04. Found: C, 53.36; H, 6.35.

***trans*-{1-naphthyl-d_7-OP(*i*-Pr)$_2$}$_2$NiBr$_2$ (3a-d_7).** 1-Naphthol-d_8 (152 mg, 1.00 mmol) was converted to the corresponding phosphinite, and all of the recovered ligand was used to prepare the title complex. Yield: 348 mg of an orange powder (0.462 mmol, 92%).

***trans*-{2-CH$_3$CD$_2$-1-naphthyl-OP(*i*-Pr)$_2$}$_2$NiBr$_2$·CH$_3$CN (3d-d_2).** 2-CH$_3$CD$_2$-1-naphthol (348 mg, 2.00 mmol) was converted to the corresponding phosphinite, and all of the recovered ligand was used to prepare the title complex. Yield: 727 mg of a dark red powder (0.910 mmol, 91%).

***trans*-{3-CD$_3$-2-naphthyl-OP(*i*-Pr)$_2$}$_2$NiBr$_2$ (3f-d_3).** 3-CD$_3$-2-naphthol (322 mg, 2.00 mmol) was converted to the corresponding phosphinite, and all of the recovered ligand was used to prepare the title complex. Yield: 681 mg of a red powder (0.881 mmol, 88%).

H/D Scrambling Experiments. *In Acetonitrile.* Deuterated complexes (ca. 100 mg) were heated at 80 °C in 2 mL CH_3CN for the required time (1 or 3 days). The final mixtures were cooled down to room temperature and placed overnight in a freezer at −35 °C. The resulting crystals were collected, washed with cold CH_3CN (2 × 1.5 mL), and dried under vacuum. The material was analyzed by ^{1}H NMR in $CDCl_3$, and the integration of the incorporated protons into D positions (if any) was compared to the integration of the methyne in P(CH(CH$_3$)$_2$)$_2$ to determine the amount of protons at D positions.

In Toluene. Deuterated complexes (ca. 100 mg) were heated at 100 °C in 2 mL $C_6H_5CH_3$ for the required time (1 or 3 days). Evaporation of the solvent under a vacuum, redissolution in CH_3CN at room temperature, filtration, and cooling overnight in a freezer at −35 °C afforded crystals, which were collected, washed with cold CH_3CN (2 × 1.5 mL), and dried under vacuum. The material was analyzed by ^{1}H NMR, and the integration of the incorporated protons into D positions (if any) was compared to the integration of the methyne in P(CH(CH$_3$)$_2$)$_2$ to determine the ratio of protons at D positions.

***cis*-(κ^P,$\kappa^{P'}$-2-P(*i*-Pr)$_2$-1-naphtyl-OP(*i*-Pr)$_2$)NiBr$_2$ (4).** To a solution of 260 mg of 1-naphthyl-OP(*i*-Pr)$_2$ (1.00 mmol) in 4 mL acetonitrile was added 288 mg of {(*i*-PrCN)NiBr$_2$}$_n$ (0.50 mmol, 0.50 equiv). This gave a red mixture containing an orange precipitate of **3a** which was subsequently heated at 200 °C for 1 h in the Monowave 50. The resulting dark red solution was evaporated, and the residues were treated in 6 mL toluene and filtered to remove the insoluble residues. Evaporation of the filtrate gave a red, sticky material that was redissolved in 3 mL acetonitrile, filtered and placed in a freezer at −35 °C for 48 h. The red crystals were isolated and washed with cold acetonitrile (3 × 1.5 mL) and dried under vacuum to give 56 mg of crystalline material. ^{1}H NMR (500 MHz, 20 °C, C_6D_6) δ 1.00−1.14 (m, 12H, C1$_{Ar}$−OP[CH(CH_3)(CH$_3$)]$_2$ and C2$_{Ar}$−P[CH(CH_3)-(CH$_3$)]$_2$), 1.40 (dd, 6H, C1$_{Ar}$−OP[CH(CH$_3$)(CH_3)]$_2$, $^3J_{HH}$ = 6.9, $^3J_{HP}$ = 16.8), 1.66 (dd, 6H, C2$_{Ar}$−P[CH(CH$_3$)(CH_3)]$_2$, $^3J_{HH}$ = 7.0, $^3J_{HP}$ = 15.7), 2.61 (hept, 2H, C2$_{Ar}$−P[CH(CH$_3$)$_2$]$_2$, $^3J_{HH}$ = 7.0), 2.83 (oct, 2H, C1$_{Ar}$−OP[CH(CH$_3$)$_2$]$_2$, $^3J_{HH} \approx {}^2J_{HP}$ = 7.2), 6.93 (d, 1H, C3$_{Ar}$−H, $^3J_{HH}$ = 8.2), 7.19 (d, 1H, C4$_{Ar}$−H, $^3J_{HH}$ = 8.7), 7.21−7.26 (m, 2H, C6$_{Ar}$−H and C7$_{Ar}$−H), 7.46−7.52 (m, 1H, C5$_{Ar}$−H), 8.03−8.09 (m, 1H, C8$_{Ar}$−H). ^{13}C{^{1}H} NMR (125.7 MHz, 20 °C, C_6D_6) δ 18.80 (s, 2C, C1$_{Ar}$−OP[CH(CH$_3$)(CH$_3$)]$_2$ or C2$_{Ar}$−P[CH(CH$_3$)-(CH$_3$)]$_2$), 18.86 (s, 2C, C1$_{Ar}$−OP[CH(CH_3)(CH$_3$)]$_2$ or C2$_{Ar}$−P[CH(CH_3)(CH$_3$)]$_2$), 20.04 (s, 2C, C1$_{Ar}$−OP[CH(CH$_3$)(CH$_3$)]$_2$), 21.00 (s, 2C, C2$_{Ar}$−P[CH(CH$_3$)(CH$_3$)]$_2$), 26.31 (d, 2C, C1$_{Ar}$−OP[CH(CH$_3$)$_2$]$_2$, $^2J_{CP}$ = 27.7), 34.50 (d, 2C, C2$_{Ar}$−P[CH(CH$_3$)$_2$]$_2$, $^2J_{CP}$ = 26.5), 122.86 (d, 1C, C4$_{Ar}$−H), 122.96 (d, 1C, C8$_{Ar}$−H), 126.57 (d, 1C, C3$_{Ar}$−H), 127.41 (d, 1C, C6$_{Ar}$−H or C7$_{Ar}$−H), 128.26 (s, 1C, C5$_{Ar}$−H, hidden under the peak for C_6D_6), 129.12 (s, 1C, C6$_{Ar}$−H or C7$_{Ar}$−H), 135.98 (s, 1C, C2$_{Ar}$−P), 157.20 (s, 1C, C1$_{Ar}$−OP). ^{31}P{^{1}H} NMR (202.4 MHz, 20 °C, C_6D_6) δ 29.33 (d, 1P, C2$_{Ar}$−P, 64.8), 176.77 (d, 1P, C1$_{Ar}$−OP, 65.4).

(*i*-Pr$_2$PH)$_2$NiBr$_2$. To a solution of 288 mg of 2-Et-1-naphthyl-OP(*i*-Pr)$_2$ (1.00 mmol) in 4 mL acetonitrile was added 316 mg of {*i*-PrCN)NiBr$_2$}$_n$ (1.10 mmol, 1.10 equiv). The resulting dark greenish solution that contained a red precipitate of **3d** was heated at 160 °C for 1 h in the Monowave 50. The resulting emerald green solution was left to stand at room temperature for 1 h during which time a pale green precipitate formed. The solution was separated by filtration and

DOI: 10.1021/acs.organomet.9b00660
Organometallics XXXX, XXX, XXX−XXX

kept overnight in a −35 °C freezer to give red crystals and some additional precipitate $\{NiBr_2(MeCN)_x\}_n$. The latter was removed by washing the solid residues with 3 × 2 mL H_2O, and the water was removed by washing with 3 × 1.5 mL cold acetonitrile. After drying under vacuum, 44 mg of red crystals were collected. While the crystal structure discloses the *cis* isomer of the complex (with a solid state ^{31}P NMR with δ 30.34 ppm, see Figure S122), the solution NMR of the complex in C_6D_6 is rather in accordance with the *trans* isomer, as proven by the correlation between the experimental spectrum and the simulation realized with a $^{v}J_{P-H}$ coupling constant of 300−400 Hz. ^1H NMR (500 MHz, 20 °C, C_6D_6) δ 1.09 (br s, 12H, $CH(CH_3)(CH_3)$), 1.50 (br s, 12H, $CH(CH_3)(CH_3)$), 2.07 (br s, 4H, $CH(CH_3)_2$), 3.79 (br m, 2H, P-*H*, ^{v}J = 345). $^{13}C\{^1H\}$ NMR (125.7 MHz, 20 °C, C_6D_6) δ 20.59 (s, $CH(CH_3)(CH_3)$), 21.25 (s, $CH(CH_3)(CH_3)$), 21.98 (br s, $CH(CH_3)_2$). $^{31}P\{^1H\}$ NMR (202.4 MHz, 20 °C, C_6D_6) δ 41.74.

■ ASSOCIATED CONTENT

Supporting Information

The Supporting Information is available free of charge at https://pubs.acs.org/doi/10.1021/acs.organomet.9b00660.

Additional synthetic procedures, NMR spectra; additional ORTEPs/figures and crystallographic details (PDF)

Accession Codes

CCDC 1952151−1952167 contain the supplementary crystallographic data for this paper. These data can be obtained free of charge via www.ccdc.cam.ac.uk/data_request/cif, or by emailing data_request@ccdc.cam.ac.uk, or by contacting The Cambridge Crystallographic Data Centre, 12 Union Road, Cambridge CB2 1EZ, UK; fax: +44 1223 336033.

■ AUTHOR INFORMATION

Corresponding Author

*E-mail: zargarian.davit@umontreal.ca.

ORCID

Davit Zargarian: 0000-0002-0207-7007

Notes

The authors declare no competing financial interest.

■ ACKNOWLEDGMENTS

The authors gratefully acknowledge financial support provided by NSERC of Canada (Discovery grants to D. Z.); Centre in Green Chemistry and Catalysis (CGCC/CCVC, summer research stipends and travel awards); Université de Montréal (graduate scholarships to L. P. M.). We also thank our colleague, Dr. Pedro Aguiar, for his availability and discussions upon NMR related topics, for ^{31}P solid state NMR of compounds **3f** and $(i\text{-}Pr_2PH)_2NiBr_2$ and simulation of the ^1H NMR spectrum of the latter.

■ REFERENCES

(1) (a) Kakiuchi, F.; Kochi, T. Transition-Metal-Catalyzed Carbon-Carbon Bond Formation via Carbon-Hydrogen Bond Cleavage. *Synthesis* **2008**, *2008* (19), 3013−3039. (b) Ackermann, L. Carboxylate-Assisted Transition-Metal-Catalyzed C−H Bond Functionalizations: Mechanism and Scope. *Chem. Rev.* **2011**, *111* (3), 1315−1345. (c) Yamaguchi, J.; Yamaguchi, A. D.; Itami, K. C−H Bond Functionalization: Emerging Synthetic Tools for Natural Products and Pharmaceuticals. *Angew. Chem., Int. Ed.* **2012**, *51* (36), 8960−9009. (d) Ackermann, L. Metal-catalyzed direct alkylations of (hetero)arenes via C−H bond cleavages with unactivated alkyl halides. *Chem. Commun.* **2010**, *46* (27), 4866−4877. (e) Chen, D. Y. K.; Youn, S. W. C−H Activation: A Complementary Tool in the Total Synthesis of Complex Natural Products. *Chem. - Eur. J.* **2012**, *18* (31), 9452−9474.

(2) (a) Klei, S. R.; Tan, K. L.; Golden, J. T.; Yung, C. M.; Thalji, R. K.; Ahrendt, K. A.; Ellman, J. A.; Tilley, T. D.; Bergman, R. G. C−H Bond Activation by Iridium and Rhodium Complexes: Catalytic Hydrogen−Deuterium Exchange and C−C Bond-Forming Reactions. In *Activation and Functionalization of C−H Bonds*; American Chemical Society, 2004; Vol. *885*, pp 46−55. (b) Colby, D. A.; Bergman, R. G.; Ellman, J. A. Rhodium-Catalyzed C−C Bond Formation via Heteroatom-Directed C−H Bond Activation. *Chem. Rev.* **2010**, *110* (2), 624−655. (c) Rouquet, G.; Chatani, N. Catalytic Functionalization of C(sp2)−H and C(sp3)−H Bonds by Using Bidentate Directing Groups. *Angew. Chem., Int. Ed.* **2013**, *52* (45), 11726−11743. (d) Arockiam, P. B.; Bruneau, C.; Dixneuf, P. H. Ruthenium(II)-Catalyzed C−H Bond Activation and Functionalization. *Chem. Rev.* **2012**, *112* (11), 5879−5918. (e) Lyons, T. W.; Sanford, M. S. Palladium-Catalyzed Ligand-Directed C−H Functionalization Reactions. *Chem. Rev.* **2010**, *110* (2), 1147−1169. (f) Xu, L.-M.; Li, B.-J.; Yang, Z.; Shi, Z.-J. Organopalladium(iv) chemistry. *Chem. Soc. Rev.* **2010**, *39* (2), 712−733. (g) Sehnal, P.; Taylor, R. J. K.; Fairlamb, I. J. S. Emergence of Palladium(IV) Chemistry in Synthesis and Catalysis. *Chem. Rev.* **2010**, *110* (2), 824−889.

(3) (a) Castro, L. C. M.; Chatani, N. Nickel Catalysts/N,N′-Bidentate Directing Groups: An Excellent Partnership in Directed C−H Activation Reactions. *Chem. Lett.* **2015**, *44* (4), 410−421. (b) Gandeepan, P.; Müller, T.; Zell, D.; Cera, G.; Warratz, S.; Ackermann, L. 3d Transition Metals for C−H Activation. *Chem. Rev.* **2019**, *119* (4), 2192−2452. (c) Beattie, D. D.; Grunwald, A. C.; Perse, T.; Schaefer, L. L.; Love, J. A. Understanding Ni(II)-Mediated C(sp3)-H Activation: Tertiray Ureas as Model Substrates. *J. Am. Chem. Soc.* **2018**, *140*, 12602−12610. (d) Roy, P.; Bour, J. R.; Kampf, J. W.; Sanford, M. S. Catalytically Relevant Intermediates in the Ni-Catalyzed C(sp2)−H and C(sp3)−H Functionalization of Aminoquinoline Substrates. *J. Am. Chem. Soc.* **2019**, *141*, 17382−17387.

(4) Vabre, B.; Deschamps, F.; Zargarian, D. Ortho Derivatization of Phenols through C−H Nickelation: Synthesis, Characterization, and Reactivities of Ortho-Nickelated Phosphinite Complexes. *Organometallics* **2014**, *33* (22), 6623−6632.

(5) Mangin, L. P.; Zargarian, D. C−H nickellation of phenol-derived phosphinites: regioselectivity and structures of cyclonickellated complexes. *Dalton Transactions* **2017**, *46* (46), 16159−16170.

(6) Mangin, L. P.; Zargarian, D. C−H Nickelation of Aryl Phosphinites: Mechanistic Aspects. *Organometallics* **2019**, *38* (7), 1479−1492.

(7) Bedford, R. B.; Limmert, M. E. Catalytic Intermolecular Ortho-Arylation of Phenols. *J. Org. Chem.* **2003**, *68* (22), 8669−8682.

(8) Satoh, T.; Inoh, J.-i.; Kawamura, Y.; Kawamura, Y.; Miura, M.; Nomura, M. Regioselective Arylation Reactions of Biphenyl-2-ols, Naphthols, and Benzylic Compounds with Aryl Halides under Palladium Catalysis. *Bull. Chem. Soc. Jpn.* **1998**, *71* (9), 2239−2246.

(9) This compound was prepared in-house. For synthetic details see the SI.

(10) It should be noted here that a lower H-incorporation had been observed with the $C_6D_5OPR_2$ analogue mentioned above, indicating a smoother reaction with **1a-*d*$_7$**.

(11) For instance, C−H nickelation of 3-R-$C_6H_4OP(i\text{-}Pr)_2$ occurs at C6 either exclusively (R = Me, Cl, OMe, NMe_2) or predominantly (R = F; C6:C1= 6:1). Moreover, C−H nickelation is facilitated by electron-releasing substituents. Similar observations were made in the case of phosphinites derived from 3,5-R_2-phenols: C−H nickelation does not take place at all with R = Me and Cl, whereas with R = OMe it does proceed, albeit very sluggishly. See ref 6 for these results.

(12) The impact of substituent electronics on C−H nickelation has also been probed in the case of pincer-type ligands featuring two donor moieties such as phosphinites or phosphines. See these reports for details: (a) Vabre, B.; Lambert, M. L.; Petit, A.; Ess, D. H.; Zargarian, D. Nickelation of PCP- and POCOP-Type Pincer Ligands: Kinetics and Mechanism. *Organometallics* **2012**, *31* (17), 6041−6053. (b) Castonguay, D.; Spasyuk, N.; Madern, A. L.; Beauchamp;

DOI: 10.1021/acs.organomet.9b00660
Organometallics XXXX, XXX, XXX−XXX

Zargarian, D. Regioselective Hydroamination of Acrylonitrile Catalyzed by Cationic Pincer Complexes of Nickel(II). *Organometallics* **2009**, *28*, 2134−2141.

(13) The contention that the C1 position is more electron-rich is based on literature reports on the greater reactivity of this site in the Claisen rearrangement, a reaction that is more sensitive to electronic as opposed to steric factors. For instance, the rearrangement of *O*-allyl-2-naphthol takes place with a C1:C3 regioselectivity of 98:2: Gozzo, F. C.; Fernandes, S. A.; Rodrigues, D. C.; Eberlin, M. N.; Marsaioli, A. J. Regioselectivity in Aromatic Claisen Rearrangements. *J. Org. Chem.* **2003**, *68* (14), 5493−5499.

(14) These values were derived by applying the following equation $\tau_4 = \{360 - (\alpha + \beta)\}/141$, wherein α and β are the largest bond angles in the given structure. This approach generates values ranging from 0 for an ideal square plane to 1 for an ideal tetrahedron. For a discussion of this topic, see the following reports: (a) Yang, L.; Powell, D. R.; Houser, R. P. Structural variation in copper(i) complexes with pyridylmethylamide ligands: structural analysis with a new four-coordinate geometry index, τ4. *Dalton Transactions* **2007**, 955−964. (b) Rosiak, D.; Okuniewski, A.; Chojnacki, J. Copper(I) iodide ribbons coordinated with thiourea derivative. *Acta Crystallogr., Sect. C: Struct. Chem.* **2018**, *74* (12), 1650−1655.

(15) The mounted crystal of **2g** was found to be a 2-component twin and the Br ligand was found disordered in both the complexes of the asymmetric unit.

(16) (a) Spasyuk, D. M.; Gorelsky, S. I.; van der Est, A.; Zargarian, D. Characterization of Divalent and Trivalent Species Generated in the Chemical and Electrochemical Oxidation of a Dimeric Pincer Complex of Nickel. *Inorg. Chem.* **2011**, *50* (6), 2661−2674. (b) Lefèvre, X.; Spasyuk, D. M.; Zargarian, D. New POCOP-Type Pincer Complexes of Nickel(II). *J. Organomet. Chem.* **2011**, *696* (4), 864−870.

(17) In contrast, control experiments showed no decomposition at 160 °C for the free phosphinite **1a** or the cyclonickelated product **2a**.

(18) Quantification of this C−H nickelation reaction was done by integrating the ^{31}P singlet at 192 ppm against the signal for $[n\text{-Bu}_4\text{N}][\text{PF}_6]$ used as an internal standard.

(19) The major resonances present in the $^{31}\text{P}\{^1\text{H}\}$ NMR spectrum of this mixture were the same as in the spectrum for the analogous reaction with 1 equiv of **1a** (i.e., AB doublets arising from compound **4** and the singlet at 121 ppm), but in this case we observed an additional minor resonance, a set of doublets at 167 and 150 ppm with $J \approx 27$ ppm.

(20) Recall that isolation and full characterization of phosphinite adducts of the cyclonickelated complexes has been reported previously: See ref 4.

(21) For primary reports and a review describing this type of reactivity see the following sources: (a) Abdellah, I.; Lepetit, C.; Canac, Y.; Duhayon, C.; Chauvin, R. Imidazoliophosphines are True N-Heterocyclic Carbene (NHC)−Phosphenium Adducts. *Chem. Eur. J.* **2010**, *16* (44), 13095−13108. (b) Abdellah, I.; Boggio-Pasqua, M.; Canac, Y.; Lepetit, C.; Duhayon, C.; Chauvin, R. Towards the Limit of Atropochiral Stability: H-MIOP, an N-Heterocyclic Carbene Precursor and Cationic Analogue of the H-MOP Ligand. *Chem. Eur. J.* **2011**, *17* (18), 5110−5115. (c) Vabre, B.; Canac, Y.; Duhayon, C.; Chauvin, R.; Zargarian, D. Nickel(II) Complexes of the New Pincer-Type Unsymmetrical Ligands PIMCOP, PIMIOCOP, and NHCCOP: Versatile Binding Motifs. *Chem. Commun.* **2012**, *48* (84), 10446−10448. (d) Vabre, B.; Canac, Y.; Lepetit, C.; Duhayon, C.; Chauvin, R.; Zargarian, D. Charge Effects in PCP Pincer Complexes of Ni^{II} bearing Phosphinite and Imidazol(i)ophosphine Coordinating Jaws: From Synthesis to Catalysis through Bonding Analysis. *Chem. Eur. J.* **2015**, *21* (48), 17403−17414. (e) Canac, Y. Carbeniophosphines versus Phosphoniocarbenes: The Role of the Positive Charge. *Chem. Asian J.* **2018**, *13* (15), 1872−1887.

(22) Monitoring the thermal profile of this reaction revealed an exothermic reaction as soon as it reached 150 °C.

(23) It is worth noting that the ^{1}H NMR (C_6D_6) spectrum of $(i\text{-Pr}_2\text{PH})_2\text{NiBr}_2$ crystals indicated that it adopts a *trans* conformation in solution: simulations established that the broadened multiplet detected at ca. 3.79 ppm for the P−*H* protons arises from a virtual coupling with *trans* P nuclei featuring $^{v}J_{\text{PH}}$ of 300−400 Hz.

(24) Complete crystallographic data for all compounds structurally characterized in this study, including the molecular diagrams not included here, are presented in the Supporting Information.

(25) (a) Ng, J. K.-P.; Tan, G.-K.; Vittal, J. J.; Leung, P.-H. Optical Resolution and the Study of Ligand Effects on the Ortho-Metalation Reaction of Resolved (±)-Diphenyl[1-(1-naphthyl)ethyl]phosphine and Its Arsenic Analogue. *Inorg. Chem.* **2003**, *42* (23), 7674−7682. (b) Ding, Y.; Chiang, M.; Pullarkat, S. A.; Li, Y.; Leung, P.-H. Synthesis, Coordination Characteristics, Conformational Behavior, and Bond Reactivity Studies of a Novel Chiral Phosphapalladacycle Complex. *Organometallics* **2009**, *28* (15), 4358−4370. (c) Li, X.-R.; Yang, X.-Y.; Li, Y.; Pullarkat, S. A.; Leung, P.-H. Efficient access to a designed phosphapalladacycle catalyst via enantioselective catalytic asymmetric hydrophosphination. *Dalton Transactions* **2017**, *46* (4), 1311−1316. (d) Li, X.-R.; Chen, Y.; Pang, B. P.; Tan, J.; Li, Y.; Pullarkat, S. A.; Leung, P.-H. Efficient Synthesis of Malonate Functionalized Chiral Phosphapalladacycles and their Catalytic Evaluation in Asymmetric Hydrophosphination of Chalcone. *Eur. J. Inorg. Chem.* **2018**, *2018* (39), 4385−4390.

(26) (a) Cloutier, J.-P.; Zargarian, D. Functionalization of the Aryl Moiety in the Pincer Complex (NCN)NiIIIBr2: Insights on NiIII-Promoted Carbon−Heteroatom Coupling. *Organometallics* **2018**, *37* (9), 1446−1455. (b) Cloutier, J.-P.; Rechignat, L.; Canac, Y.; Ess, D. H.; Zargarian, D. C−O and C−N Functionalization of Cationic, NCN-Type Pincer Complexes of Trivalent Nickel: Mechanism, Selectivity, and Kinetic Isotope Effect. *Inorg. Chem.* **2019**, *58* (6), 3861−3874.

(27) Obermayer, D.; Znidar, D.; Glotz, G.; Stadler, A.; Dallinger, D.; Kappe, C. O. Design and Performance Validation of a Conductively Heated Sealed-Vessel Reactor for Organic Synthesis. *J. Org. Chem.* **2016**, *81* (23), 11788−11801.

(28) (a) Vabre, B.; Spasyuk, D. M.; Zargarian, D. Impact of Backbone Substituents on POCOP-Ni Pincer complexes: A Structural, Spectroscopic and Electrochemical Study. *Organometallics* **2012**, *31* (24), 8561−8570. (b) Vabre, B.; Lindeperg, F.; Zargarian, D. Direct, one-pot synthesis of POCOP-type pincer complexes from metallic nickel. *Green Chem.* **2013**, *15* (11), 3188−3194.

DOI: 10.1021/acs.organomet.9b00660
Organometallics XXXX, XXX, XXX−XXX